Fluorescence Based Quantification of Messenger RNA and Plasmid DNA Decay Kinetics in Extracellular Biological Fluids and Cell Extracts

Heyang Zhang[1], Koen Rombouts[1], Laurens Raes[1,2], Ranhua Xiong[1,2], Stefaan De Smedt[1,2]*, Kevin Braeckmans[1,2]*, Katrien Remaut[1]*

Affiliations:

[1]Laboratory of General Biochemistry and Physical Pharmacy, Faculty of Pharmaceutical Sciences, Ghent University, 9000 Ghent, Belgium

[2]Centre for Nano- and Biophotonics, Ghent University, 9000 Ghent, Belgium

Corresponding authors:

Katrien.Remaut@UGent.be; Kevin.Braeckmans@UGent.be; Stefaan.Desmedt@UGent.be;

Prof. Katrien Remaut will handle correspondence at all stages of refereeing and publication, also post-publication.

Tel: +32 9 264 80 76, Fax: +32 9 264 81 89

Corresponding address:

Ottergemsesteenweg 460, 9000 Ghent, Belgium

Keywords: nucleic acids, extracellular and intracellular degradation, FCS, SPT

Abstract

Extracellular and intracellular degradation of nucleic acids remains an issue in non-viral gene therapy. Understanding biodegradation is critical for the rational design of gene therapeutics, in order to maintain stability and functionality at the target site. However, there are only limited methods available that allow to determine the stability of genetic materials in biological environments. In this context, we studied the decay kinetics of fluorescently labeled pDNA and mRNA in undiluted biological samples (i.e. human serum, human ascites, bovine vitreous) and cell extracts by using Fluorescence Correlation Spectroscopy (FCS) and Single Particle Tracking (SPT). We demonstrate that FCS is suitable to follow mRNA degradation, while SPT is better suited to investigate pDNA integrity. The half-life of mRNA and pDNA was approximately 1-2 min and 1 to 4 h in biological samples, respectively. The resistance against biodegradation drastically improved by complexation with lipid-based carriers. Taken together, FCS and SPT are able to quantify the integrity of respectively mRNA and pDNA as a function of time, both in the extracellular biological fluids and cell extracts. This on its turn allows us to focus on the important but less understood issue of nucleic acids degradation in more detail and to rationally optimize gene delivery system as therapeutics.

Introduction

Since the completion of the Human Genome Project in 2003, many disease-causing genes were identified, sparking the interest for gene therapy[1–5]. In gene therapy, nucleic acids, including plasmid DNA (pDNA), messenger RNA (mRNA), small interfering RNA (siRNA) and antisense oligonucleotides (AONs) are delivered into the patient's cells, with the aim to overrule or correct the gene defect that lies at the root of the disease[6]. The delivery of nucleic acids to target cells remains however problematic, as nucleic acids by themselves do not efficiently cross cell membranes. To guide them into the intracellular environment, the negatively charged nucleic acids are often complexed with a cationic carrier (e.g. cationic lipids or polymers) to improve cellular uptake and enhance endosomal escape. Furthermore, as changes in the sequence of nucleic acids will abolish their therapeutic effect, the carrier system should protect the nucleic acids against degradation during all steps of the delivery process[7].

Studying the degradation of nucleic acids in a representative extracellular and intracellular environment is very relevant but highly challenging, as there are only limited methods that allow to measure this degradation *in situ*. To date, the stability of nucleic acids is often studied by gel electrophoresis. This technique, however, does not allow to measure degradation directly in crowded biologic environments, as the presence of free nucleic acids and other biomolecules overrules the signal of the therapeutic nucleic acid of interest[8]. Alternatively, Polymerase Chain Reaction (PCR) has been utilized to study the cytoplasmic degradation of nucleic acids with high sensitivity and specificity[9]. There are however limitations as well, including costly kits and reagents, contamination chances, and most importantly, the need to isolate nucleic acids that rules out *in situ* analysis and complicates time-dependent analysis[10].

To follow degradation of nucleic acids *in situ*, mostly fluorescence microscopy-based methods are used. In Fluorescence *In Situ* Hybridization (FISH), a fluorescent probe is used to bind the target DNA or RNA with high specificity, based on sequence complementarity. Trcek *et al*. for example, utilized

two-color RNA FISH to characterize the temporal and spatial non-sense mediated mRNA decay and showed the co-existence of two populations with distinct half-life (< 1 min and > 12 h) within the same cells[11]. FISH was also applied by Lechardeur *et al*. to study the metabolic instability of pDNA in the cytosol, finding a half-life of about 90 min[12]. However, FISH is mainly applied in fixed cells, where possible effects of the fixation on the nucleic acid distribution or denaturation can't be ruled out. Moreover, some of the relatively short FISH probes may non-specifically bind to endogenous nucleic acids, thus leading to the false positive results. As well, most FISH probes are shorter than the whole length of the nucleic acids they are binding, especially mRNA, it is unclear how larger degradation products (that might still contain the target sequence) can be distinguished from intact sequence. Taken together, FISH is not straightforward to follow the intracellular degradation of nucleic acids as a function of time[13].

To provide dynamic information on the nucleic acids' fate, methods are needed that allow for non-invasive measurements in living cells. The group of K. Leong applied a two-step quantum dot Fluorescence Resonance Energy Transfer (FRET) approach, to simultaneously and non-invasively analyze DNA condensation and stability in living cells[14]. Santangelo's group, on the other hand, developed a single RNA sensitive fluorescent labeling method to elegantly study mRNA uptake and release kinetics from endocytic compartments on a single cell level[15]. Our group has demonstrated previously that Fluorescence Correlation Spectroscopy (FCS) allows to follow the intracellular degradation of short nucleic acids like AONs and siRNA in living cells, as a function of time[16–20]. FCS is a real-time fluorescence technique that records the continuous movement of fluorescent molecules in and out of a confocal detection volume, allowing to provide quantitative data on their concentration and diffusion coefficient[21]. Due to its single-molecule sensitivity, and the possibility for *in situ* measurements, FCS has been used to study many biological questions, such as ligand-receptor interactions, protein folding, decay rates, association and dissociation kinetics and so on[22,23]. The suitability of FCS to follow the degradation of large nucleic acids like mRNA and pDNA, has however not been evaluated before. In this chapter, we evaluated the potential of FCS to follow the integrity of

large nucleic acids like mRNA and pDNA, based on a change in diffusion rate between intact and degraded fragments. We additionally evaluated another fluorescence microscopy-based technique, namely Single Particle Tracking (SPT), to explore the stability of nucleic acids based on a change in diffusional behavior upon degradation. As the name implies, SPT is developed to track individual mobile fluorescent particles or molecules in time and space by mapping their individual trajectories in time-lapse videos. Then, diffusion coefficient (or size) and concentration of the tracked fluorescent objects can be calculated. SPT is mostly suitable to track molecules or particles with a size above 0.1 µm, or diffusion coefficient of 0.0001-10 $\mu m^2 \cdot s^{-1}$[24]. Our group has demonstrated that SPT is ideally suited to characterize the mobility and aggregation of nanoparticles in biological fluids (plasma, blood and ascites fluid), extracellular matrices (lung mucus and vitreous humor) as well as for intracellular trafficking[25–30]. Therefore, we hypothesized that SPT has the potential to 'track' the degradation of mRNA and pDNA in extracellular and intracellular environments as well. Both FCS and SPT were tested in a step by step approach: first, we tested the ability to quantify the number of intact nucleic acids in buffer. Then, we studied pre-formed mixtures of intact and degraded fractions of nucleic acids, before proceeding to nuclease-mediated degradation in buffer as a function of time. Next, the decay kinetics of mRNA and pDNA were followed in undiluted biological samples, both in their naked form as well as complexed by a non-viral lipid-based carrier. Finally, the intracellular degradation of nucleic acids in Hela cells and SKOV-3 cells was determined after delivery through lipofection (complexed nucleic acids) and nucleofection (free nucleic acids) by the determination of intact mRNA and pDNA fragments in cell lysates.

Results

Quantification of intact mRNA and pDNA in HEPES buffer

To determine the feasibility of FCS and SPT to measure the concentration of intact nucleic acids, first a standard curve was prepared by measuring a dilution series in HEPES buffer. Figure 1, A and B, show a representative fluorescence fluctuations and auto-correlation curve from FCS measurements on Cy5

labeled mRNA in HEPES buffer (6 μg·mL^{-1}), respectively. All correlation curves could be fitted by a 1-species fit, resulting in a diffusion coefficient of 19.5 ± 1.2 μm²·s^{-1} (supplementary Figure S3). Furthermore, as Figure 1C shows, FCS allowed to reliably determine the concentration of intact mRNA in a dilution series. Indeed, the measured mRNA concentration as determined by FCS (Y-axis, nM) was in good linearity with the expected mRNA concentration calculated from the applied dilution factor (X-axis, nM). Additionally, we tried to quantify Cy5 mRNA by SPT. Intact mRNA molecules were however never observed by SPT, showing that the mRNA (10-50 nm) applied in this study was smaller than the detection limit of SPT[24,31]. The fact that single mRNA molecules remained undetected by SPT is due to a combination of limited fluorescence per mRNA molecule (with on average 6 ± 1 labels per mRNA, supplementary Figure S1) and fast diffusional motion. As a result too little photons are captured to reliably identify an mRNA molecule over the background signal.

Next we investigated whether FCS or SPT is more suited to detect single pDNA molecules. Figure 1, D and E, show a representative fluorescence fluctuations and auto-correlation curve as obtained by FCS on an intact Cy5 labeled pDNA solution (5 μg·mL^{-1}). Interestingly, pDNA displayed fluorescence peaks in the fluorescence fluctuation profile (Figure 1D), which were not observed for mRNA molecules (Figure 1A). Most likely, this results from the higher labeling density of the pDNA (on average 73 ± 11 labels per pDNA, supplementary Figure S1), when compared to the linear mRNA. pDNA molecules are clearly diffusing more slowly when compared to mRNA, with an average diffusion coefficient of 3.0 ± 0.7 μm^2·s^{-1}, which is close to expectations for a 5800 bp plasmid[32]. Also for pDNA, FCS was able to quantify the expected amount of intact pDNA in the dilution series (R^2=0.9957), as demonstrated in Figure 1F. Next, the feasibility of SPT to detect pDNA was examined. As Figure 1G shows, SPT was able to detect individual plasmids, allowing the construction of individual trajectories of Cy5 pDNA (as shown in supporting information). From these trajectories, a diffusion coefficient of 2.3 ± 0.7 μm^2·s^{-1} was obtained (Figure 1H), which was in reasonable agreement with the diffusion coefficient measured by FCS. Furthermore, as Figure 1I shows, SPT allowed to quantify the number of intact pDNA molecules, giving a good linearity (R^2=0.9842) between the measured and expected pDNA concentration in the

dilution series ranging from 0.001 to 0.5 µg·mL^{-1}. For the Cy5 pDNA concentration of 1 µg·mL^{-1}, however, the identification of motion trajectories was not reliable as the high pDNA concentration hampered the detection of plasmids as individual spots[33]. Therefore, SPT only allows to reliably quantify pDNA up to a concentration of 0.5 µg·mL^{-1} in HEPES buffer.

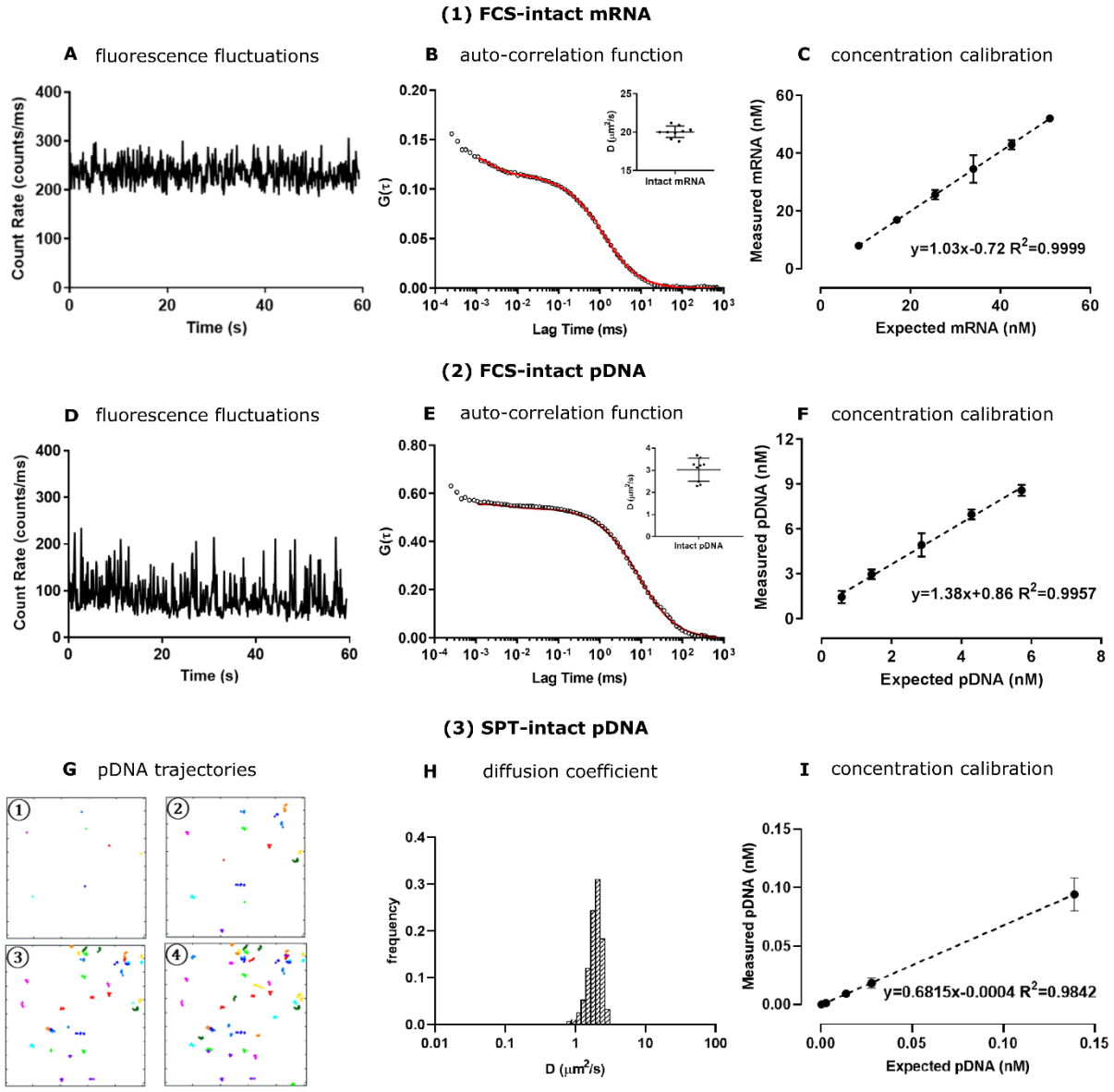

Figure 1. Quantification of (1) Cy5 mRNA and (2, 3) Cy5 pDNA in HEPES buffer. (A) Representative fluorescence fluctuations as a function of time and (B) auto-correlation function G(τ) as a function of lag time during FCS measurements of 6 µg·mL^{-1} Cy5 mRNA. (C) Cy5 mRNA was quantified by FCS and auto-correlation analysis within the range of 3-18 µg·mL^{-1}, where X and Y-axis represent the expected (nM) and measured (nM) concentration of mRNA, respectively. (D) Representative fluorescence fluctuations as a function of time and (E) auto-correlation

function G(τ) as a function of lag time during FCS measurements of 5 $\mu g \cdot mL^{-1}$ Cy5 pDNA. (F) Cy5 pDNA was quantified by FCS and auto-correlation analysis within the range of 2-20 $\mu g \cdot mL^{-1}$, where X and Y-axis represent the expected (nM) and measured (nM) concentration of pDNA, respectively. (G) Individual trajectories and representative movie of Cy5 pDNA (0.05 $\mu g \cdot mL^{-1}$) motion in HEPES buffer. By using an in house-developed program, (H) the diffusion coefficient of Cy5 pDNA and (I) the concentration calibration within the range of 0.001-0.5 $\mu g \cdot mL^{-1}$ of pDNA was quantified, where the X and Y-axis represented the expected (nM) and measured (nM) concentration of pDNA respectively. All the experiments were performed for three independent times.

FCS and SPT to distinguish intact from degraded mRNA and pDNA

The standard curves above demonstrate that intact mRNA can be quantified by FCS, while both FCS and SPT can be used to determine intact pDNA. According to Stokes-Einstein equation, the diffusion coefficient is a function of the particle diameter. When nucleic acids degrade, it is expected that faster diffusing fragments will arise. It can be seen that fully degraded mRNA and pDNA fragments indeed diffuse faster (Figure 2, B and E) when compared to their intact counterparts in Figure 1, B and E. Interestingly, the fluorescent peaks that occurred in FCS measurements of intact pDNA disappeared in the degraded samples, confirming degradation into smaller, single labeled components (Figure 1D *vs* Figure 2D). When SPT was applied on fully degraded pDNA (Figure 2G, 0% intact pDNA), fluorescent particles were no longer observed as they are too dim and move too fast to be seen as individual particles.

To evaluate whether FCS and SPT can quantify intact from degraded nucleic acids in a single solution, intact and degraded nucleic acids were mixed at known w/w ratios of 100, 80, 60, 40, 20 and 0% of intact nucleic acids with 0, 20, 40, 60, 80 and 100% of fully degraded nucleic acids, respectively. As there are two components present in the mixtures, FCS auto-correlation curves were fitted by a dual-species fit. Representative individual fittings and resulting parameters are added in the supplementary Figure S4. When both components are left free during the fitting (Figure 2C, blue line), an overestimation of the slow component is apparent from the calibration curve. When the diffusion

coefficient of the intact mRNA is fixed to 20 $\mu m^2 \cdot s^{-1}$ (Figure 2C, black line), this overestimation can be reduced, although on average 18% of false positive intact mRNA is calculated for the fully degraded sample. In the range between 40% and 100% of intact mRNA, however, the fitting is representative for the amount of intact mRNA in the mixtures. Also for pDNA, FCS was able to reliably detect the percentage of intact pDNA into the mixtures containing varying amounts of degraded pDNA fragments (Figure 2F). Again, the auto-correlation curves were best fitted with a dual-species fit (supplementary Figure S4), resulting in the percentage of intact (average diffusion coefficient of 3.8 ± 1.1 $\mu m^2 \cdot s^{-1}$) and degraded (average diffusion coefficient of 221.2 ± 36.1 $\mu m^2 \cdot s^{-1}$) pDNA.

In contrast to FCS, SPT was not able to simultaneously detect intact and degraded pDNA, as pDNA degradation fragments could no longer be tracked (Figure 2G, 0% intact pDNA). However, the amount of intact pDNA can still be quantified in the mixtures (Figure 2G), based on the relative number of trajectories that were found. As can be seen from Figure 2H, the distribution of diffusion coefficients obtained from the trajectories corresponds to intact pDNA. As Figure 2I implies, there was a good correlation between the measured and expected number of intact pDNA in the mixtures (R^2=0.9694), although there was a tendency for overestimation in samples containing 20% of intact pDNA, probably due to the diminished contrast of intact pDNA in the background of degraded fluorescent Cy5 pDNA fragments. In conclusion, both FCS and SPT were able to quantify the fraction of intact and degraded pDNA in a mixture with intact and fully degraded pDNA.

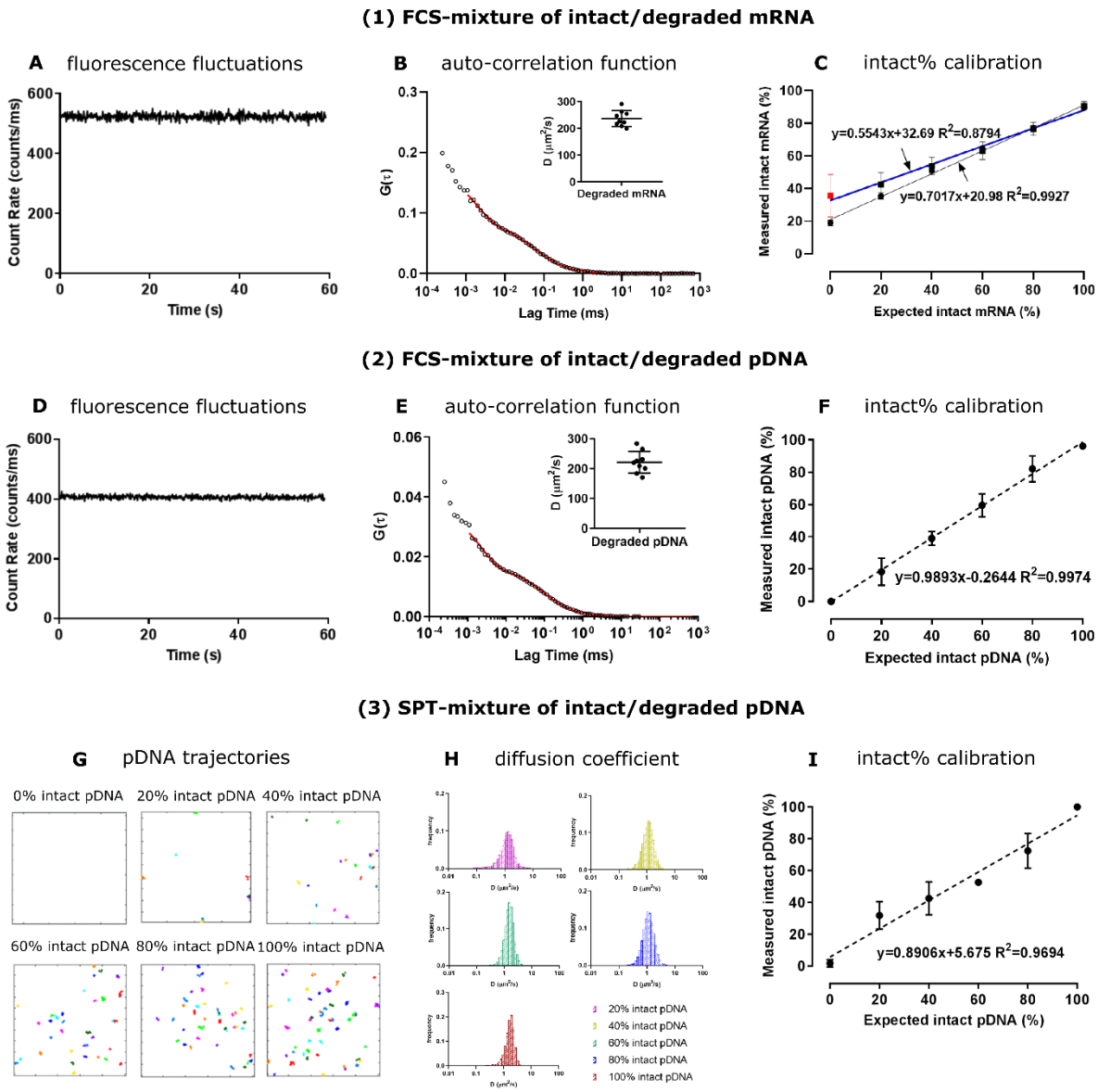

Figure 2. Quantification of (1) Cy5 mRNA and (2, 3) Cy5 pDNA in intact/degraded mixture with known w/w ratios of 0/100, 20/80, 40/60, 60/40, 80/20 and 100/0 %. (A) Representative fluorescence fluctuations over time and (B) auto-correlation function as a function of lag time during FCS measurements of fully degraded mRNA in HEPES buffer. (C) Fraction of intact Cy5 mRNA was quantified by dual-species auto-correlation analysis either by leaving both components free (blue line) or by fixing the diffusion coefficient of the slow component to 20 $\mu m^2 \cdot s^{-1}$ (black line). Red data points indicate the analysis where the dual-species fit generated a slow component with a diffusion coefficient that did not correspond to intact mRNA. (D) Representative fluorescence fluctuations over time and (E) auto-correlation function as a function of lag time during FCS measurements of fully degraded pDNA in HEPES buffer. (F) Fraction of intact pDNA was quantified by dual-species auto-correlation analysis, where diffusion of both components was left free. (G) Individual trajectories of intact/degraded Cy5 pDNA mixture. (H)

Distribution of diffusion coefficient of pDNA in the mixtures of intact/degraded pDNA. (I) Fraction of intact pDNA (%) in the mixture of intact/degraded Cy5 pDNA as quantified by SPT. All the experiments were performed for three independent times.

mRNA degradation in function of time, mediated by RNase A

After having verified that both intact and degraded mRNA can be quantified by FCS, we tested to see if was possible to use FCS to follow the degradation of mRNA mediated by RNase A as a function of time. In brief, mRNA was incubated with different amounts of RNase A at 37 °C, and at the chosen time points, an aliquot was removed, the reaction was completely inhibited by adding a RNase inhibitor and a fraction of the samples was loaded onto a 1% agarose gel, while the remaining fraction of the same samples was analyzed by FCS. From the agarose gels (Figure 3A), mRNA degradation was clearly visible as a function of time with increasing RNase A amounts (starting from 0.03 $U \cdot \mu g^{-1}$ mRNA), by the appearance of degradation fragments that run further into the agarose gel. By using Image J, the brightness of the bands corresponding to intact mRNA was quantified and the relative amount of intact mRNA (%) at t>0 was calculated by comparing with the brightness at t=0. As expected, degradation as a function of time depends on the amount of added RNase A, resulting in respectively 20%, 50% and 100% degradation for 0.01, 0.03 and 0.2 or 0.3 Unit RNase A per 1 µg of mRNA after 30 min incubation (Figure 3B).

The same samples were analyzed by auto-correlation analysis, by applying a dual-species fit. As shown in Figure 3C, the kinetics of mRNA decay were comparable to that of gel electrophoresis, with a slight difference for the 0.01 $U \cdot \mu g^{-1}$ sample. Apparently, for this low enzyme concentration, FCS gave a slight overestimation of the intact mRNA amount likely because partly degraded fragments still have a diffusion coefficient close to the intact ones. Also, degradation plateaus at 10 to 30% of intact mRNA, which is attributed to false positives created due to the dual-species fit, with D_1 fixed at 20 $\mu m^2 \cdot s^{-1}$ (supplementary Figure S4).

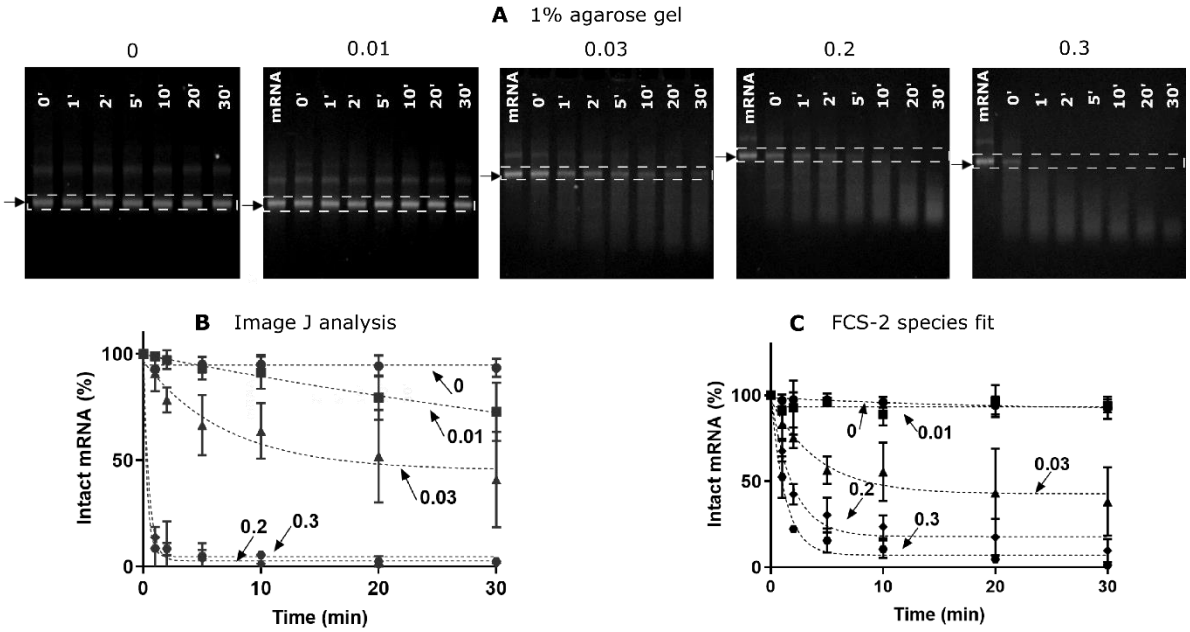

Figure 3. Cy5 mRNA degradation mediated by RNase A and quantified by 1% agarose gel electrophoresis and FCS. (A) Representative gel for mRNA decay by varying amount of RNase A (Unit per 1 μg mRNA, as showed above the images) at 37 °C for 0, 1, 2, 5, 10, 20 and 30 min, as depicted above the lanes. The level of intact mRNA is indicated by the arrow and the white squares. (B) mRNA decay kinetics over time by gel electrophoresis and analyzed by Image J, with different amount of RNase A: 0 $U \cdot \mu g^{-1}$ (circle), 0.01 $U \cdot \mu g^{-1}$ (square), 0.03 $U \cdot \mu g^{-1}$ (triangle), 0.2 $U \cdot \mu g^{-1}$ (diamond), 0.3 $U \cdot \mu g^{-1}$ (hexagon). (C) mRNA decay as a function of time with varying amount of RNase A, 0 $U \cdot \mu g^{-1}$ (circle), 0.01 $U \cdot \mu g^{-1}$ (square), 0.03 $U \cdot \mu g^{-1}$ (triangle), 0.2 $U \cdot \mu g^{-1}$ (diamond), 0.3 $U \cdot \mu g^{-1}$ (hexagon), measured by FCS and dual-species auto-correlation analysis. All experiments were performed for three independent times. Decay parameters are listed in supplementary Table 1 and 2.

pDNA degradation as a function of time, mediated by DNase I

Similarly, intact pDNA decay over time was visualized by 1% agarose gel (Figure 4A). In 30 min, no degradation was observed for 0 and 0.06 U DNase I per 1 μg pDNA, while degradation clearly occurred with 0.1, 0.2 and 0.3 $U \cdot \mu g^{-1}$ DNase I. At the 5 min time point, for example, some intact pDNA was observed for 0.1 $U \cdot \mu g^{-1}$ DNase I while intact pDNA was no longer observed for 0.2 and 0.3 $U \cdot \mu g^{-1}$. The amount of intact pDNA as a function of time was quantified by Image J (Figure 4B), FCS (Figure 4C) and SPT (Figure 4D). In general, with increasing amounts of DNase I, intact pDNA (%) decreased as a

function of incubation time. More than 50% of pDNA remained intact after 30 min incubation when less than 0.2 U DNase I was added per 1 µg of pDNA, while pDNA rapidly degraded when incubated with DNase I at 0.2 and 0.3 $U \cdot \mu g^{-1}$. When pDNA degradation as a function of time was followed by FCS (Figure 4C), the amount of intact pDNA was clearly overestimated when compared to gel electrophoresis (Figure 4B). Apparently, the mixture of all different lengths of pDNA fragments makes it impossible to reliably distinguish intact from partially degraded pDNA, based on our analysis method. When the same samples were analyzed with SPT, degradation kinetics were comparable to those observed with gel electrophoresis for samples incubated with 0 to 0.2 $U \cdot \mu g^{-1}$ pDNA, except the overestimation of intact pDNA molecules for samples incubated with 0.3 $U \cdot \mu g^{-1}$ pDNA, especially at the short time scales (e.g. 5 and 10 min) (Figure 4D). Taken together, it seems that FCS is mainly applicable to follow mRNA degradation, while pDNA degradation can be more reliably quantified by SPT, even though the fraction of intact molecules may be overestimated during the initial degradation steps.

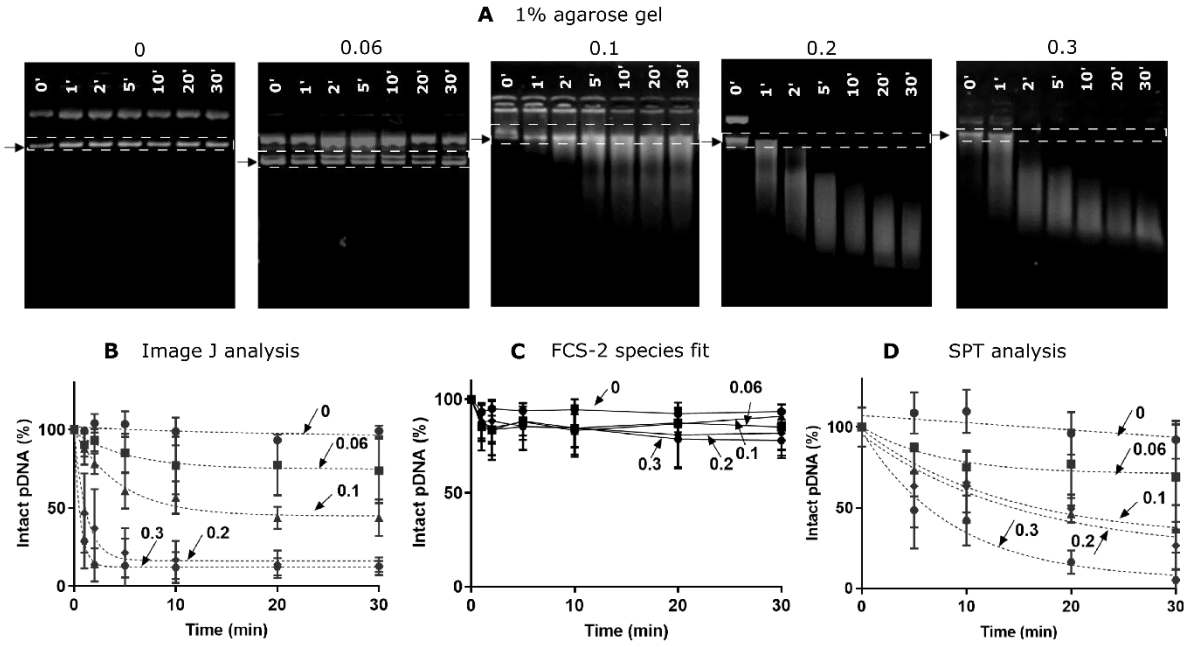

Figure 4. Cy5 pDNA degradation mediated by DNase I and quantified by 1% agarose gel electrophoresis, FCS and SPT. (A) Representative gel for pDNA decay by varying amount of DNase I (as showed above the images) at 37 °C for 0, 1, 2, 5, 10, 20 and 30 min, as depicted above the lanes. The level of intact supercoiled pDNA is indicated by the arrow and the white squares. Quantification of pDNA decay kinetics over time by gel electrophoresis and

analyzed by (B) Image J, (C) FCS and (D) SPT, with different amount of DNase I: 0 $U \cdot \mu g^{-1}$ (circle), 0.06 $U \cdot \mu g^{-1}$ (square), 0.1 $U \cdot \mu g^{-1}$ (triangle), 0.2 $U \cdot \mu g^{-1}$ (diamond), 0.3 $U \cdot \mu g^{-1}$ (hexagon). All experiments were performed for three independent times. Decay parameters are listed in supplementary Table 3 and 4.

mRNA and pDNA degradation in undiluted biological samples

Intravenous administration, intraperitoneal delivery as well as intravitreal injection have potential for mRNA and pDNA delivery[34–36]. The decay kinetics of administrated nucleic acids (especially mRNA) in blood (or serum, plasma), peritoneal fluid and vitreous, which is crucial to optimize gene delivery systems and their administration routes, however are not well-understood. Therefore, we followed the degradation of mRNA and pDNA in undiluted biological samples, namely human serum, human ascites and bovine vitreous. Again, degradation as a function of time was evaluated by gel electrophoresis (for both mRNA and pDNA), FCS (for mRNA) and SPT (for pDNA). As can be seen from Figure 5, A (mRNA) and B (pDNA), both human serum and human ascites give a strong background signal on the agarose gel, hampering reliable quantification of the fraction of intact molecules. Bovine vitreous, on the other hand, does not interfere with the readout of the gels. It should be noted that it takes around 5 min to prepare and then load samples on the agarose gel, explaining while most of the mRNA was degraded already on the t=0 time point (Figure 5A), which also confirms the limitation of gel electrophoresis to follow nucleic acids degradation. FCS analysis of mRNA degradation (Figure 5C) shows that mRNA was rather stable in HEPES buffer at room temperature, but rapidly degraded in the presence of biological samples. Indeed, already after 5 min of incubation, less than 50% of intact mRNA remained, revealing an estimated half-life of around 1-2 min only. Again, degradation decay plateaus at 10 to 30% of intact mRNA, which is attributed to false positives created due to the dual-species fit, with D_1 fixed at 20 $\mu m^2 \cdot s^{-1}$ (supplementary Figure S5). When SDS was added to the biological samples as nuclease inhibitor, more than 90% of mRNA remained intact during incubation in human serum and human ascites (3% SDS) and bovine vitreous (0.5% SDS) (supplementary Figure S6, A)[37].

SPT analysis of pDNA degradation revealed that pDNA was more stable in human serum than human ascites and bovine vitreous (Figure 5D). Indeed, after 8 hours' incubation in human ascites and bovine vitreous, more than 90% of pDNA degraded into small fragments, whereas around 80% of pDNA remained intact in human serum and HEPES buffer. It should be noted that the amount of intact pDNA also decreased slightly in HEPES buffer, where no nucleases are expected to be present. The loss of pDNA over time may indicate that intact pDNA has the tendency to stick to the wall of the polypropylene eppendorf tubes (Sorenson™, BioScience Inc.) in which incubation was performed, thereby lowering the free diffusing concentration of pDNA as a function of time[38]. Interestingly, we found no significant decrease of intact pDNA (%) in HEPES buffer when 3% SDS was present during the 8 h incubation (supplementary Figure S6, B), demonstrating that sticking of pDNA on the wall of eppendorf tubes was prevented. As SDS also effectively inactivates nucleases present in the biological samples (supplementary Figure S7), however, SDS was only added at the end of the incubation period when degradation was followed as a function of time[39].

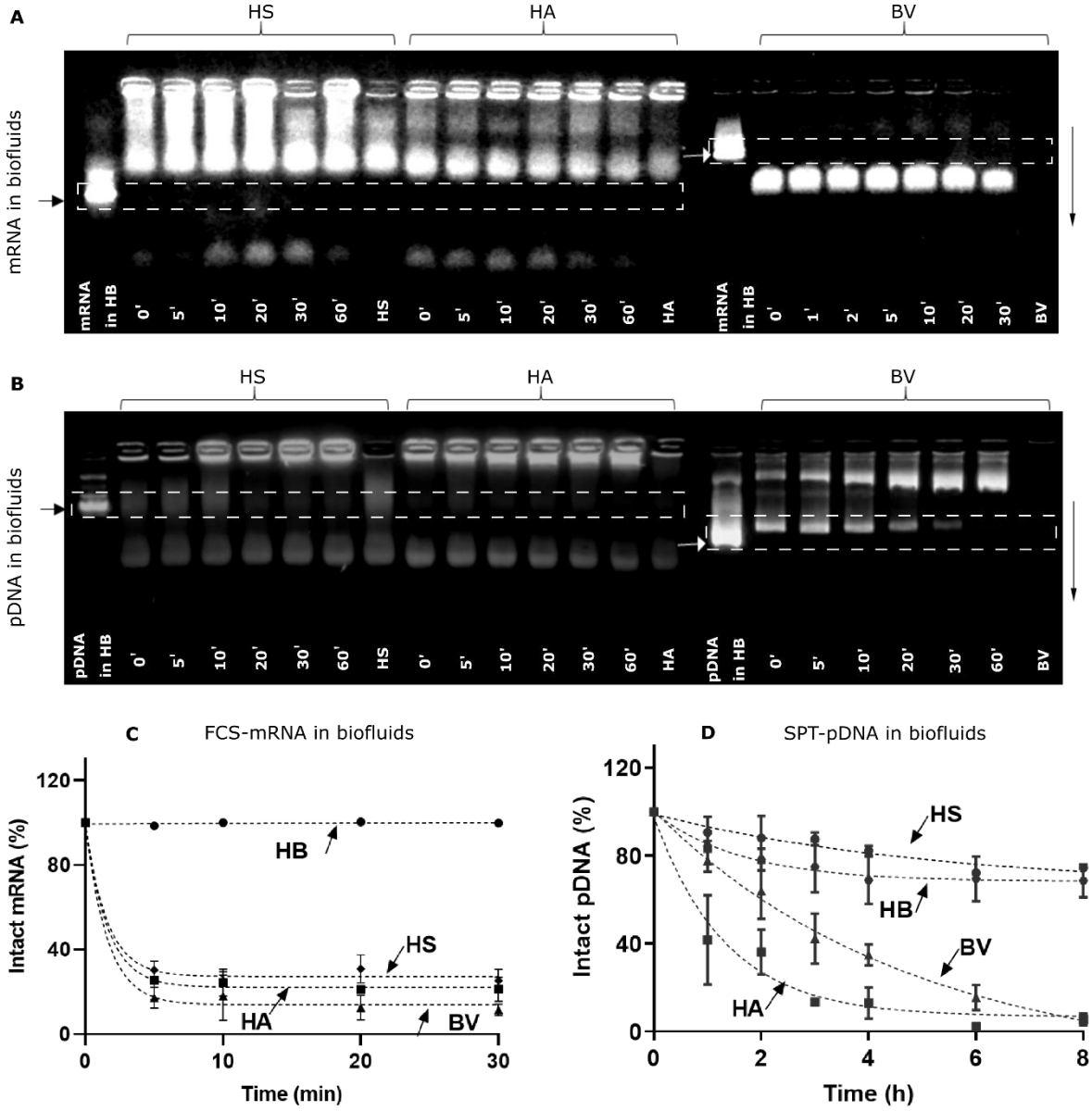

Figure 5. (A-B) Representative gel of mRNA (A) and pDNA (B) degradation in HEPES buffer (HB, as control), human serum (HS), human ascites (HA) and bovine vitreous (BV) as a function of time at 37 °C. The arrow and white squares indicate the level of intact mRNA and supercoiled pDNA, respectively. (C) Quantification of mRNA decay in HB (circle), HS (diamond), HA (square) and BV (triangle) at 37 °C for 0, 5, 10, 20, 30 min as determined by FCS. (D) Quantification of Cy5 pDNA degradation in HB (circle), HS (diamond), HA (square) and BV (triangle) at 37 °C for 0, 1, 2, 3, 4, 6 and 8 h as determined by SPT. All experiments were performed for three independent times. Decay parameters are listed in supplementary Table 5 and 6.

Next, we evaluated whether the degradation of mRNA and pDNA in the biological samples could be prevented by complexing them with commercial lipid-based carriers, namely mMax and LF2000 for

mRNA and pDNA, respectively. Therefore, complexes were incubated in the biological samples and at the chosen time points, a small aliquot was removed and SDS was added to inhibit the nuclease activity while simultaneously releasing the mRNA and pDNA from the complexes to allow for the quantification of the intact nucleic acids by FCS and SPT, respectively, as shown in supplementary Figure S8[37,40,41]. As Figure 6A demonstrates, almost 100% of mRNA remained intact in HEPES buffer, both in naked and complexed form, demonstrating the feasibility of the method. In the biological samples, complexed mRNA was degrading as a function of time, although it should be noted that the half-life of mRNA increased from minutes to several hours when mRNA was present in the complexed form (supplementary Table 5). For plasmid DNA, the situation is more complex (Figure 6B). When SPT is used to analyze the intact amount of pDNA as a function of time, the apparent amount of intact pDNA decreases in all cases, leaving the impression that complexed pDNA is less protected against degradation when compared to its free form (Figure 5D). As the fraction of intact pDNA also decreases in the control situation (HEPES buffer without nucleases), however, this decrease does not result from degradation. Most likely, the aggregation and sticking of complexes to the wells lead to a loss of detectable pDNA, as these complexes will remain in the stock solution, and will not be present in the sampled aliquots that were measured. Based on the comparison with human serum, without nuclease activity, however, we can confirm that complexation by LF2000 offers additional protection to the pDNA.

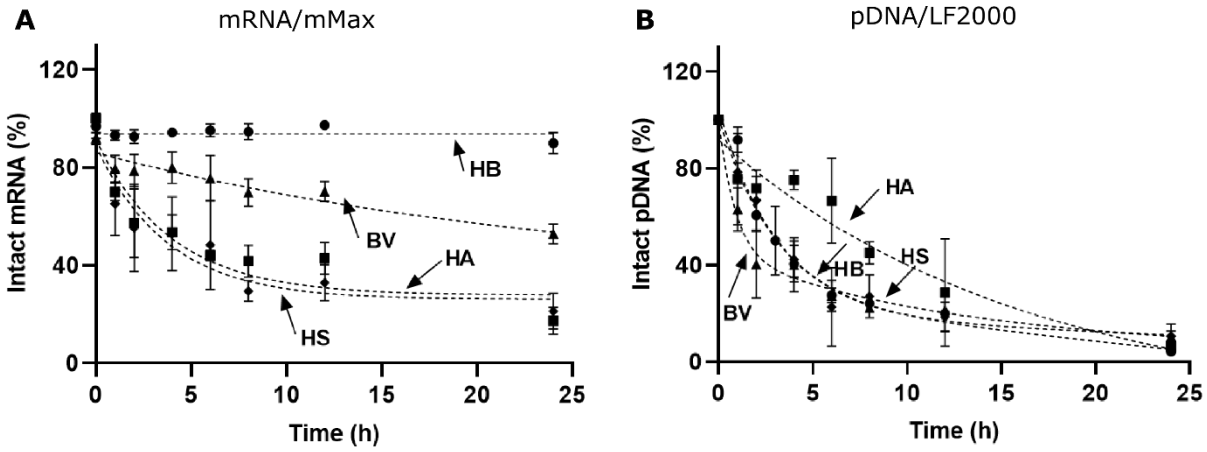

Figure 6. Carrier mediated protection of mRNA and pDNA in biological samples. A stock solution of complexes were incubated in the HB (circle), HS (diamond), HA (square) and BV (triangle) and at the chosen time points, a small aliquot was removed and SDS was added with a final concentration of 3% and incubated at room temperature for 20 min before performing (A) FCS measurements for mRNA and (B) SPT analysis for pDNA, respectively. All the experiments were performed for three independent times. Decay parameters are listed in supplementary Table 5 and 6.

Intracellular degradation of mRNA and pDNA after lipofection and nucleofection

In the next set of experiments, we tested the decay kinetics of mRNA and pDNA once delivered into the cells in 'complexed' and 'naked' form. Therefore, mRNA or pDNA was complexed with mMax and LF2000, respectively, at a v/w ratio of 3 according to the protocol from the manufacturer. Then, the resulting complexes were added to Hela cells and SKOV-3 cells to allow for uptake and endocytosis of the lipid-based carriers (e.g. lipofection). Alternatively, naked nucleic acids were delivered to the cells by nucleofection, which is assumed to directly transfer them into the cytoplasm or nucleus of cells, although there may be a contribution by endocytic uptake as well[42]. At the end of incubation or nucleofection, cell lysate was prepared and SDS was added to inhibit nuclease activity and dissociate mRNA and pDNA from the complexes prior to FCS and SPT measurements, respectively. The quantity of intact molecules was set to 100% as a relative starting point at the first measured time point, which was immediately after nucleofection (t=0 h) and 4 hours after transfection (to allow for cellular uptake of the complexed mRNA and pDNA). After that, as Figure 7, A and B show, mRNA gradually degraded over time both when delivered in its 'naked' and 'complexed' form, independent of the cell type. The degradation of mRNA in its naked form, however, seems to proceed faster when compared to the complexed form, confirming the vector's capability of protecting genetic payloads from biodegradation. In analogy, pDNA was delivered into Hela cells and SKOV-3 cells by lipofection and nucleofection. Unexpectedly, naked pDNA degraded rather rapidly in both Hela cells and SKOV-3 cells (Figure 7C) when compared to mRNA (Figure 7A). Interestingly, more pDNA remained intact when

delivered in its complexed form by lipofection, demonstrating again the protection of the nucleic acids by the lipid-based carriers during intracellular delivery.

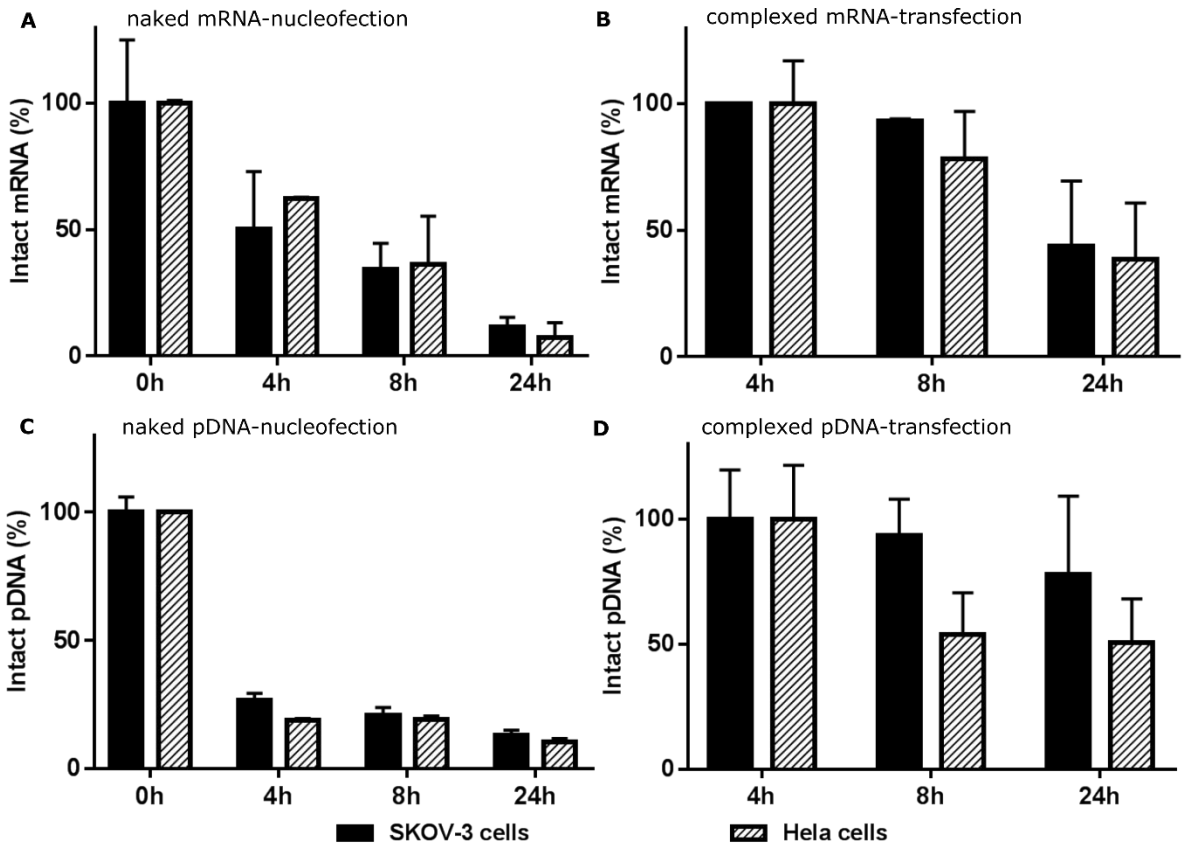

Figure 7. Intracellular degradation of mRNA (A, B) and pDNA (C, D) delivered in naked form by nucleofection (A, C) and complexed form (B, D) by mMax (v/w ratio of 3) and LF2000 respectively in SKOV-3 cells (black bar) and Hela cells (striped bar) At the end of incubation, mRNA or pDNA treated cells were lysed and SDS was then added to the cell lysate to inhibit nuclease activity and release complexed mRNA or pDNA before performing measurements. All the experiments were performed for three independent times.

Discussion

Various pathologies such as cancer and genetic diseases are characterized by a dysregulated gene expression. The ability to specifically overexpress certain proteins (by mRNA or pDNA delivery) or to silence gene expression (by antisense oligonucleotides or siRNA) is an interesting therapeutic strategy to manipulate gene expression levels in the target cells. Nucleic acids can be delivered as such, or when complexed to viral or non-viral gene delivery systems. As the nucleic acid sequence is crucial to

maintain biological activity, degradation during the different steps of the delivery pathway is highly undesirable. The extent to which degradation of nucleic acids in the extracellular and intracellular environments is a barrier in gene therapy, remains however largely understudied, also because of a lack of suitable methods to follow degradation *in situ*. Gel electrophoresis is commonly used to follow the degradation of nucleic acids in buffer (such as PBS, HEPES buffer, etc.) and simplified culture medium (normally with 10% FBS) by visualization of the intact and degraded nucleic acids on the gel. Gel electrophoresis is, however, not applicable to follow degradation in biological samples such as blood and cell extracts due to the high background signal of macromolecules present in the biological samples. PCR is a highly specific technique to detect nucleic acids extracted from biological context, with high sensitivity (as low as pictogram). However, several practical issues, such as false positive or negative results, the need for nucleic acids extraction and time-consuming amplification (around 2 h), decreases the chance of PCR to follow nucleic acids degradation, especially for the large nucleic acids with long sequence. In contrast to PCR, fluorescence-based techniques, in this context, FCS and SPT, are able to quickly (within a few minutes) quantify the real-time degradation of mRNA and pDNA respectively, with minimal sample preparation and protocol optimization. In this study, we explored to which extent FCS and SPT are suited to measure the extracellular and intracellular biodegradation of mRNA and pDNA, respectively.

mRNA is a single stranded ribonucleic acid that should reach the cytoplasm of the cells to induce protein expression. mRNA has long been perceived as being too unstable for gene delivery applications[43]. Due to advances in delivery systems and modifications to the mRNA backbone, mRNA use has boomed in the past few years[44]. The mRNA used in this work (996 nucleotides, M_W of 353 kDa), could not be quantified by SPT. As SPT relies on the visibility of individual fluorescent particles, this indicates that the labeled mRNA, which contains on average 6 labels per molecule, did not provide enough fluorescent photons to be imaged reliably as a separate entity within the short illumination time (30 ms) of a single frame. This is further complicated by the fast diffusion of mRNA that causes motion blur. FCS, however, does not rely on imaging particles but rather integrates the entire

fluorescent signal from the confocal volume on a single-photon sensitive point detector as a function of time. By analyzing the fluorescence intensity fluctuations over time, FCS was very well able to determine the concentration of intact mRNA in a simple dilution series based on single species fit to the auto-correlation curve. Intact mRNA had a diffusion coefficient of around 20 $\mu m^2 \cdot s^{-1}$ (Figure 1B, inset), corresponding to a hydrodynamic diameter of 25 nm according to the Stokes-Einstein equation. When visualized in solution, Kobler *et al.* reported a mRNA size ranging of 10-45 nm for a 975 nt long mRNA molecule, which is in line with our calculated RNA size[31]. When mRNA degraded, the diffusion coefficient increased to 239.1 ± 30.5 $\mu m^2 \cdot s^{-1}$ (Figure 2B, inset). As D is proportional to $1/(M_W)^{0.53}$ for linear molecules like mRNA, this 12 fold change in diffusion coefficient indicates a 108 fold change in M_W of the intact mRNA, indicating the breakdown into degradation products of on average 9 nucleotides[45]. Interestingly, by applying a dual-species fit on the FCS auto-correlation data, we were able to quantify intact and degraded mRNA fragments co-existing in the same solution (Figure 2C) and RNase induced mRNA degradation as a function of time (Figure 3C). With the lowest RNase concentration of 0.01 $U \cdot \mu g^{-1}$ mRNA, however, the small amount of degradation that was seen on the agarose gel (Figure 3A), was not detected by auto-correlation analysis as most likely the initial degradation fragments do not differ enough from the full-length mRNA to be distinguished by FCS (Figure 3C). In more complex biological samples, mRNA degradation was more difficult to estimate from gel electrophoresis (Figure 5A), but could be quantified by auto-correlating FCS signals in human serum, human ascites and bovine vitreous (Figure 5C). As supplementary Figure S6, A and S7 demonstrate, SDS can be used to inhibit nuclease activity present in these biological samples. The presence of SDS altered the running distance of intact mRNA in the agarose gel, but did not seem to interfere with the auto-correlation analysis of the FCS signal. Therefore, FCS clearly has an advantage over gel electrophoresis in more complex biological context. Our data demonstrates that RNases are present in all tested biological samples, which was in line with the literature[46]. Ribonuclease T2 (RNase T2), for example, was found within the ovarian stromal microenvironment[47]. The concentration of human RNase 1 in plasma was 0.4 $mg \cdot L^{-1}$, and it is also expressed in testis, ovary, brain, mammary

gland and other tissues and found in other biological samples such as urine, milk, urine, saliva and seminal plasma[48][49].

By electrostatic interactions between cationic vectors and anionic nucleic acids, complexes can be formed that are expected to protect genetic payloads from nucleases, facilitate cellular uptake and increase cytosolic mobility[50]. When mRNA was complexed to the commercial lipid-based carrier mMax, it was clearly protected against degradation in human serum, human ascites and bovine vitreous, with a half-life increasing from minutes to several hours (Figure 6, A, supplementary Table 5). The protection of mRNA against degradation also demonstrated that with mMax, about 50% of mRNA molecules are attached on the surface, while the remaining 50% is encapsulated inside the complexes. Our current data indicates that the fraction of mRNA attached on the surface of lipoplexes was still accessible for nucleases present in the biological samples, while the fraction encapsulated inside the lipoplexes was protected against nucleases.

In analogy, FCS and SPT were applied to quantify plasmid DNA degradation. Plasmids are large, double-stranded circular DNA molecules that should reach the cell nucleus to induce protein expression. pDNA can exist in the supercoiled, open circular or linear form, although we have previously demonstrated that supercoiled pDNA is the most efficient to induce protein expression[51]. Again, FCS was able to quantify a dilution series of intact pDNA, by applying single species auto-correlation. Intact pDNA had an average diffusion coefficient approximately 3.0 $\mu m^2 \cdot s^{-1}$ (Figure 1E, inset), corresponding to an average hydrodynamic size around 86 nm based on the Stokes-Einstein equation. Interestingly, fluorescence peaks occurred in the fluorescence fluctuation profiles, that were not observed for mRNA (Figure 1, D *vs* A). Most likely, this results from the higher labeling density of pDNA with on average 73 ± 11 labels per plasmid. Each time such a pDNA 'particle' passes the detection volume of the FCS instrument, a fluorescence peak is registered. Upon degradation of the pDNA (Figure 2D), these fluorescence peaks disappeared as pDNA was degraded into small fragments. From the diffusion coefficient around 220 $\mu m^2 \cdot s^{-1}$, and according to the relation between size and diffusion coefficient of

$1/(M_W)^{0.33}$ for spherical molecules, intact DNA with around 5800 bp was degraded into fragments of ~3 bp[52]. While FCS was also able to quantify the ratios in mixtures of intact pDNA and fully (DNase I) degraded pDNA by using a two-species auto-correlation analysis (Figure 2F), the fraction of intact pDNA molecules in samples that degraded as a function of time was clearly overestimated (Figure 4C). From gel electrophoresis (Figure 4A), it can be seen that upon degradation of pDNA by DNase I, initially open circular pDNA was formed. Then, open circular DNA further degraded into smaller linear degradation fragments. As we showed in previous report, FCS is able to distinguish intact supercoiled DNA from open circular DNA or partly degraded linear DNA fragments[51]. To optimize the suitability of FCS to follow pDNA degradation over time in these more complex mixtures, where a large variety of pDNA fragments were formed with different sizes, the difference in labeling density and molecular brightness between different fractions should clearly be taken into account[53,54], which was beyond the scope of the current study.

Instead, SPT turned out to be better suited for this task as intact pDNA molecules could be detected as single fluorescent particles (Figure 1, G, H and I). As Figure 1H shows, the diffusion coefficient of pDNA was approximately 2.3 ± 0.7 $\mu m^2 \cdot s^{-1}$, corresponding to particles with an average hydrodynamic size of 106 ± 36 nm according to Stokes-Einstein equation, which is comparable to the size obtained from FCS measurements (86 ± 20 nm). This is also in line with previous reports and illustrates that pDNA mainly exists in the supercoiled form[51,55–58]. Upon degradation of the pDNA, however, smaller- and thus faster- fragments were no longer detected as individual objects. Instead, they contribute to the overall background signal. Furthermore, we demonstrate that we could accurately determine the concentration of intact pDNA from SPT data in solutions containing mixtures of intact pDNA with fully degraded pDNA fragments (Figure 2I) and upon enzymatic degradation of the pDNA after DNase I nuclease activity (Figure 4D). Also in more complex biological context, SPT was applicable to detect the number of intact pDNA molecules. Figure 5D reveals that human serum was a rather friendly environment for pDNA in comparison with bovine vitreous and human ascites, with a half-life of around 4 h (supplementary Table 6). Wang *et al.* found that naked pDNA incubated with 50% serum

was degraded into small fragments in 3 h and completely disappeared from the gel in 12 h, which was more or less comparable to what we observed[59]. Kawabata *et al*., however, found a much shorter half-life of DNA in whole mouse blood of approximately 10 min, while Yao *et al*. found an estimated half-life time of 30.8 min of human genomic DNA in serum[60,61]. It should be noted that the pDNA decay kinetics by nucleases are affected by its size (or length) and topology. For example, supercoiled pDNA is more stable than open circular and linear pDNA, and shorter DNA is more sensitive to degradation due to the less ectopic sites[62]. Also, Zagorovsky *et al.* reported a significant influence of serum type on DNA degradation, with around 10 times slower degradation in human compared to mouse serum[63]. In comparison with serum, pDNA degradation in bovine vitreous and human ascites is clearly rapid. In vitreous, we found that more than 90% of pDNA gradually degraded into small fragments after 8 h incubation (Figure 5D), indicating moderate DNase or topoisomerase activity in the bovine vitreous. From gel electrophoresis (Figure 5B), it can be seen that pDNA changed from supercoiled to open circular during 1 hour incubation. This is in agreement with Pitkä *et al.* who observed the change in DNA form after 2.5 h and a complete pDNA degradation after incubation for 24 h[64] and Peeters *et al.* who also found a conversion of the supercoiled pDNA to circular pDNA after incubation in bovine vitreous[65]. Clearly, pDNA degraded most quickly in human ascites, with a half-life of 0.9 h. Human ascites can occur in patients suffering from peritoneal carcinomatosis. Although pDNA has already been applied in the treatment of peritoneal cancer, this degradation of pDNA in human ascites was not reported before[66]. Interestingly, complexation of pDNA into the commercial lipid-based carrier (i.e. LF 2000) protected the pDNA from degradation in serum, human ascites and bovine vitreous at the 1 h time point (Figure 6D), again demonstrating that encapsulation can protect nucleic acids against enzymes present in the extracellular fluids. When SPT is to be used to follow the protection of complexed pDNA as a function of time, however, aggregation and/or sticking of complexes might complicate the analysis, leading to a non-degradation related decrease in intact pDNA molecules (Figure 6B). Therefore, the appropriate controls should always be taken into account for these type of measurements.

In the final set of experiments, mRNA and pDNA degradation was followed in cell lysate, obtained from cells that were transfected by lipofection or nucleofection. In lipofection, cells are incubated with lipoplexes that are taken up by endocytosis, should escape the endosomes and release their nucleic acids into the cytoplasm of the cells[67]. Once entering the cells, the genetic payload is subjected to degradation in endosomes/lysosomes, and the small fraction that may escape is exposed to further cytoplasmic degradation[68–71]. Degradative enzymes are active in late endosomes, but are more concentrated in lysosomes[72–74]. For example, RNase T2 and DNase II are well-known lysosomal endonucleases, and cleave single-stranded RNA and double-stranded DNA at an acid pH, respectively[75,76]. In nucleofection, naked nucleic acids are assumed to be directly transferred to the cytoplasm or nucleus of the cells, thereby surpassing potential degradation in the endosomal compartment. As observed from Figure 7, B and D, however, lipofection always results in higher amounts of intact nucleic acids when compared to nucleofection (Figure 7, A and B). The high protection of mRNA and pDNA in the first 8 hours following lipofection indicates the protection of the nucleic acids in the endosomal compartment due to complexation into the lipid-based carriers. This is in rough agreement with the observation from Leohardt *et al.* who found an average mRNA half-life of approximately 11 h after lipofection[77]. The observed degradation of mRNA and pDNA at the 24 h time point most likely results from the accumulative endosomal escape, releasing free nucleic acids into the cytoplasm of the cells. Interestingly, Kirschman *et al.* found that endosomal uptake starts 10-30 min after transfection, while a significant increase of free mRNA in the cytosol is observed 5 h post-transfection upon lipofection, illustrating release from the endosomes[15]. Also for pDNA, our results are well-consistent with the reported half-life of 50-90 min^{-1} by Lechardeur *et al.*[12]. Surprisingly, at each time-point more intact mRNA remains when compared to pDNA, both after lipofection and nucleofection. Therefore, it seems that mostly the existence of RNases in the extracellular environment can result in a rapid degradation of the mRNA employed in this study, while pDNA is more susceptible to intracellular degradation[78]. Also, the possibility of false positives (e.g. degradation fragments binding to higher-order structures) or false negatives (e.g. pDNA concentration decreasing

due to sticking or aggregation) should be kept in mind for these cell lysate analyses (supplementary Figure S9). It should be noted, however, that false positive intact mRNA or pDNA was barely detected in the biological fluids (supplementary Figure S5).

Also for the *in situ* follow up of intracellular pDNA and mRNA degradation, some limitation of the current proposed methods should be taken into account. With SPT, it is difficult to separate the signal from pDNA in complexes and in endosomal compartments from the intact pDNA in the cytoplasm of the cells. Moreover, as SPT concentration measurements are based on the assumption of 3D free diffusion of fluorescent molecules (or particles), it won't be reliable of there is hindered (crowded cytoplasm) and/or confined (endosomes) diffusion. And again, degradation fragments might bind to higher order structures, leading to the detection of seemingly 'intact' molecules. As also FCS relies on the diffusion of fluorescently labeled molecules, this can be hampered in the crowded intracellular environment as well. Therefore, intracellular analysis of diffusion coefficients to follow degradation is more complicated when compared to cell lysate or buffer solutions. A solution to this problem could be the use of dual fluorescently labeled mRNA or pDNA molecules, for which both colors move together as long as the nucleic acids are intact, and move separately when degradation occurs. Double labeled mRNA, with for example a green fluorophore on the 5' end and a red fluorophore on the 3' end, would be an interesting future option to follow mRNA degradation by cross-correlation analysis, when compared to the single-colored FCS applied in this study[15,79]. Kinjo and Sasaki for example investigated the biodegradation of double labeled linear DNA (Cy5 and Rhodamine green) by using fluorescence cross correlation spectroscopy and found that mostly exonucleases instead of endonucleases degraded linear DNA in the cytoplasm[80]. Also, the possibility to use pulsed interleaved excitation and the possibility to separate different species with the same color during FCS experiments based on their fluorescence lifetime, rather than diffusional analysis, could overcome the current limitation of the presented analysis method[23,53]. Finally, as both FCS and SPT rely on the measurement of fluorescently labeled molecules, one should take care to investigate that the labeling method does not interfere with the process under investigation[81]. We have shown before, for example, that

fluorescent labels increase the hydrophobicity of pDNA molecules, thereby altering endosomal escape and dissociation from lipid based carriers[82]. When taking into account the appropriate controls, however, both FCS and SPT prove to be reliable methods to measure the amount of intact mRNA and pDNA in varying environments, for which the analysis by gel electrophoresis is hampered due to too high background signals.

Conclusions

In this study, we evaluated fluorescence microscopy-based methods to study the real-time biodegradation of mRNA and pDNA in buffer, undiluted biological samples and cell extracts, and found that FCS and SPT were suitable to follow mRNA and pDNA degradation, respectively. Both methods were fast, sensitive and reliable with minimal amount of sample needed (hundreds of nanogram) and minimal sample preparation. Furthermore, both methods were applicable in biological fluids, with no to limited background signal (supplementary Figure S5) unlike the typically used gel electrophoresis. The half-life of naked mRNA in all biological samples tested (human serum, human ascites and bovine vitreous) was approximately 1-2 min, while DNA was more stable in serum when compared to bovine vitreous and human ascites. Cationic lipids-based vectors, mMax and LF2000, protected genetic payloads from extracellular degradation, with more than 50% of mRNA and 80% of pDNA remaining intact after 1 h incubation in biological samples, respectively. Also intracellular, the half-life of mRNA and pDNA increased when delivered to cells into the complexed form (*via* lipofection) when compared to naked nucleic acid delivery through nucleofection. Overall, we found that naked mRNA was rapidly degraded in extracellular fluids, while pDNA seemed more susceptible to intracellular degradation. As both FCS and SPT are based on diffusion measurements, however, there is a potential risk for overestimation of intact nucleic acids when degradation fragments bind to slowly diffusing macromolecules in extracellular and intracellular fluids. Also, the presence of a variety of different length degradation products, with varying molecular brightness can complicated the FCS analysis. In the future, these issues could be resolved by using double-labeled nucleic acids that degrade into

single-labeled fragments, combined with colocalization (SPT) or cross-correlation (FCS) analysis. Alternatively, the possibility to use pulsed interleaved excitation and the possibility to separate different species during FCS experiments based on their fluorescence lifetime could be explored.

Experimental section

Materials

Cy5-labeled non-modified messenger RNA encoding for Enhanced Green Fluorescence Protein (EGFP mRNA) was purchased from Trilink BioTechnologies (San Diego, CA, USA). RNase A (40 $U \cdot \mu L^{-1}$), RiboLock RNase inhibitor, DNase I (2 $U \cdot \mu L^{-1}$), Lipofectamine™ messengerMax and Lipofectamine™ 2000 were purchased from Thermo Fisher Scientific (Merelbeke, Belgium). HEPES, Tris-HCl, EDTA, sodium dodecyl sulfate, potassium acetate, magnesium chloride and potassium iodide and RIPA buffer (1×) were purchased from Sigma-Aldrich (Overijse, Belgium). gWIZ-GFP plasmids, expressing the green fluorescent protein (GFP) were purchased from Genlantis (San Diego, CA, USA). The plasmids were amplified in *Escherichia coli* and isolated from the bacteria suspension by using Qiafilter Plasmid Giga Kit (Qiagen, Venlo, The Netherlands). DNA concentration and purity were determined by UV absorption at 260/280 nm with NanoDrop 2000c (Thermo Fisher Scientific, Rockford, IL, USA). The plasmids were suspended in 20 mM HEPES buffer (pH7.2) at a final concentration of 1 $\mu g \cdot \mu L^{-1}$. Fluorescent labeling by Cy5 was performed using the Label-IT nucleic acid labeling kit (Mirus Bio, Madison, WI, USA) at a Label-IT: pDNA ratio of 2:1 (v/w) according to the protocol provided by the manufacturer. Labeling intensity of the mRNA and pDNA was calculated based on UV spectroscopy and FCS analysis, as demonstrated in supplementary Figure S1. Human serum was obtained from healthy volunteers. Blood was collected at Ghent University hospital and centrifuged for 10 min with a speed of 4000× g at 20 °C. Then the supernatant (serum) was aliquoted (50 µL) in sterile polypropylene tubes and stored at -20 °C and thawed at 4 °C overnight prior to use. Human ascites was obtained from patients diagnosed with peritoneal carcinomatosis at the department of medical oncology, Ghent University hospital, with approval of the ethics committee of the Ghent University

hospital (ECD no. 2013/589). Bovine vitreous was separated from bovine eyes bought in the slaughterhouse, and sonicated for 1 min at 10% amplitude with on/off of 30 s by tip sonication prior to use.

Feasibility of FCS and SPT to quantify intact mRNA and pDNA in HEPES buffer

To determine the feasibility of FCS and SPT to quantify intact nucleic acids, firstly a standard curve of mRNA and pDNA was prepared. Therefore, intact Cy5 labeled mRNA was diluted in 25 mM HEPES buffer (pH7.4) to a final concentration of 3, 6, 9, 12, 15 and 18 $\mu g \cdot mL^{-1}$ for FCS measurements, while Cy5 labeled pDNA was diluted in 20 mM HEPES buffer (pH7.2) to a final concentration of 2, 5, 10, 15 and 20 $\mu g \cdot mL^{-1}$ for FCS measurements and 0.001, 0.005. 0.01, 0.05, 0.1, 0.5 and 1.0 $\mu g \cdot mL^{-1}$ for SPT measurements. Of these samples, 50 µL and 5 µL were used for FCS and SPT measurements, respectively.

Then, mRNA and pDNA were intentionally degraded to obtain 'fully degraded' samples. Cy5 labeled mRNA was incubated with endoribonuclease RNase A (0.3 Unit RNase A per 1 µg mRNA) at 37 °C overnight. At the end of incubation, 40 $U \cdot \mu L^{-1}$ RiboLock RNase inhibitor was added to the 'degraded' mRNA followed by incubation on ice for 20 min. Cy5 labeled pDNA was incubated with endonuclease DNase I (0.3 Unit DNase I per 1 µg pDNA) in 'degradation buffer' (20 mM HEPES, 110 mM K-acetate and 2 mM Mg-acetate, pH7.4) at 37 °C overnight. After incubation, the degradation was inhibited by the addition of TBE buffer (10.8 $g \cdot L^{-1}$ Tris base, 5.5 $g \cdot L^{-1}$ boric acid and 0.58 $g \cdot L^{-1}$ EDTA) at room temperature for 20 min. To estimate the feasibility of FCS and SPT to quantify intact and degraded fragments, mixtures were prepared containing intact/degraded mRNA (or pDNA) in the w/w ratio of 0/100, 20/80, 40/60, 60/40, 80/20 and 100/0%.

Kinetics of mRNA and pDNA degradation mediated by nucleases

To follow mRNA degradation as a function of time, 0, 0.01, 0.03, 0.2, 0.3 Unit of RNase A were added per 1 µg mRNA in HEPES buffer (25 mM, pH7.4). These stock samples were incubated at 37 °C and at

each time point (0, 1, 2, 5, 10, 20 and 30 min) an 40 µL aliquot was taken, degradation was stopped by adding 10 µL RNase A inhibitor (final concentration of 1 $U \cdot mL^{-1}$) and the 50 µL aliquot (5 $\mu g \cdot mL^{-1}$ mRNA) was measured by FCS. Likewise, pDNA solutions were incubated with DNase I at 0, 0.06, 0.1, 0.2, 0.3 Units per 1 µg pDNA in degradation buffer at 37 °C. At each time point (0, 1, 2, 5, 10, 20 and 30 min) a 5 µL aliquot was taken, degradation was stopped by adding an equal volume of TBE buffer, and 5 µL of the pDNA solution (0.05 $\mu g \cdot mL^{-1}$) was transferred for SPT measurements. As control, for each time point also 25 µL solution was sampled (containing 200 ng of mRNA or pDNA) and mixed with 5 µL loading buffer to run on a 1% agarose gel at 100 V for 30 min, prior to imaging. It should be noted that also *in situ* measurements of mRNA and pDNA degradation are possible, without aliquotation.

mRNA and pDNA degradation in biological samples

A 200 times dilution of Cy5 mRNA (1.0 $\mu g \cdot \mu L^{-1}$) and a 100 times dilution of Cy5 pDNA (0.005 $\mu g \cdot \mu L^{-1}$) in biological samples (i.e. human serum, human ascites, bovine vitreous), was incubated at 37 °C during varying time points. At each time point, mRNA and pDNA solutions were sampled as above, resulting in 50 µL (5 $\mu g \cdot mL^{-1}$) mRNA solution and 5 µL (0.05 $\mu g \cdot mL^{-1}$) pDNA solution for FCS and SPT measurements, respectively. Again, also 25 µL (200 ng of mRNA or pDNA) sample was taken for each time point, mixed with 5 µL loading buffer and loaded on 1% agarose gel. To inhibit nuclease activity in biological samples, a final concentration of 3% SDS was added. The 1% agarose gel was run for 30 min at 100 V before imaging.

Alternatively, mRNA and pDNA were first complexed with Lipofectamine™ messengerMax (mMax) and Lipofectamine™ 2000 (LF2000), respectively, at a v/w ratio of 3:1 (µL/µg). The resulting lipoplexes were diluted 5 times in the biological samples (final vol. of 80%) and the stock solution was incubated at 37 °C. At each time point (0, 1, 2, 4, 6, 8, 12 and 24 h), a 40 µL (or 8 µL) aliquot was taken and 10 µL (or 2 µL) of 15% SDS was added (resulting in final concentration of 3%) and incubated for 20 min at room temperature, to inhibit nuclease activity and dissociate the mRNA (or pDNA) from the lipoplexes prior to FCS (or SPT) measurements. To examine the dissociation of mRNA and pDNA from

mMax/mRNA and LF2000/pDNA respectively, complexes were incubated with 3% SDS (final concentration) at room temperature for 20 min, followed by 1% agarose gel electrophoresis at 100 V, for 30 min.

Intracellular degradation of mRNA and pDNA

Hela cells were cultured in DMEM/F-12 with 2 mM glutamine, 10% fetal bovine serum (FBS, Hyclone), and 100 $U \cdot mL^{-1}$ penicillin/streptomycin. SKOV-3 cells were grown in McCoy's 5A medium, supplemented with 10% FBS and penicillin-streptomycin with final concentration of 2 $U \cdot mL^{-1}$. Cells with 80%-90% confluency were detached from the bottom of cell culture flask with 0.25% trypsin/EDTA. Cells were maintained in an incubator at 37 °C in a humidified atmosphere containing 5% CO_2.

For transfection experiments, Hela cells and SKOV-3 cells were seeded on 24-well plates (50,000 cells/well) 1 day before use. At v/w ratio of 3:1 (μL/μg), lipoplexes of mMax/mRNA (0.50 μg of mRNA), or LF2000/pDNA (0.17 μg of pDNA) were added to each well, and incubated at 37 °C, 5% CO_2 for 4, 8 and 24 h. After 4 hour's incubation, cells were rinsed by DPBS[-] twice and cultured in fresh culture medium. At the end of incubation, the harvested cells were centrifuged at 1100 rpm for 5 min. Then, the cell pellet was washed by DPBS [-] and cells were lysed with 0.1 mL RIPA buffer (1×) on ice for 30 min. Afterwards, the cell lysate was centrifuged at 18,000 g for 10 min at 4 °C. 10 μL of 15% SDS was added to 40 μL of supernatant containing mMax/mRNA, while an equal volume of 15% SDS was incubated with the supernatant containing LF2000/pDNA, for 20 min at room temperature to inhibit nuclease activity and dissociate the nucleic acids from the complexes prior to FCS and SPT measurements.

For nucleofection, naked mRNA (25 μg, 1.0 $\mu g \cdot \mu g^{-1}$), or naked pDNA (2.5 μg, 0.1 $\mu g \cdot \mu L^{-1}$) was diluted with 225 μL cell suspension (containing 2.6×10^6 cells) in Opti-MEM. Then, 20 μL (i.e. 2.0 μg mRNA, or 0.2 μg pDNA for 2×10^5 cells) was used for nucleofection by 4D-Nucleofector (Lonza Bioscience, Bornem, Belgium) and the nucleofected cells were incubated at 37 °C, 5% CO_2 for 0, 4, 8 and 24 h. After

4 h, the cells were rinsed twice by DPBS [-], and incubated in Opti-MEM until the expected time point. At the end of incubation, cell lysate was prepared as described above and kept at -80 °C prior to use.

Methods

Fluorescence Correlation Spectroscopy (FCS)

FCS is a minimally invasive fluorescence technique capable of detecting single molecules. Briefly, the continuous movement of fluorescent molecules in and out of the detection volume of a confocal microscope induces fluorescence fluctuations that are recorded by sensitive avalanche photo diode detectors. Based on these fluorescence fluctuations, an auto-correlation curve G(τ) is derived from which the average number of fluorescent molecules (N) and their diffusion coefficient can be determined. To do so, a single species fit is applied when only 1 type of fluorescent molecule is present (e.g. intact nucleic acids OR degraded fragments). Alternatively, a dual species fit can be applied when two populations of fluorescent molecules are expected with distinct diffusion times (e.g. intact nucleic acids AND degraded fragments) for which both the fraction of each component and their diffusion coefficient can be determined. It should be noted that for optimal distinction between subpopulations, a difference in diffusion coefficient of more than 2 (indicating a molecular weight change with factor 8) were suggested for auto-correlation analysis[83].

In our setup, FCS measurements were performed with a Nikon C1 confocal microscope, equipped with a photon counting instrument (PicoHarp 300, PicoQuant). The FCS instrument was calibrated with free Alexa 647 fluorophore, leading to a detection volume (V_{eff}) of 0.99 ± 0.05 fL using Eq.1 [53]. Fluorescence time traces were obtained during 60 s by focusing a 640 nm laser line through a water immersion objective lens (60x Plan Apo VC, N.A. 1.2, Nikon, Japan) at about 50 µm above the glass bottom of 96-well plate. The resulting auto-correlation curves were then fitted by a Triplet-state single-species (Eq.2) or dual-species (Eq.3) model using the SymPhoTime software.

$$V_{eff} = \pi^{\frac{3}{2}} {w_0}^2 z_0 \qquad \text{Eq.1}$$

$$G(t) = \frac{1}{N(1-T)} \cdot \left[1 - T + T \cdot \exp\left(\frac{-t}{\tau_t}\right)\right] \cdot \frac{1}{1+\frac{t}{\tau_t}} \cdot \frac{1}{\sqrt{1+\left(\frac{\omega_0}{z_0}\right)^2 \cdot \left(\frac{t}{\tau_1}\right)}} \qquad \text{Eq.2}$$

$$G(t) = \frac{1}{N(1-T)} \cdot \left[1 - T + T \cdot \exp\left(\frac{-t}{\tau_t}\right)\right] \cdot \left[\frac{y}{\left(1+\frac{t}{\tau_{t1}}\right)\sqrt{1+\left(\frac{\omega_0}{z_0}\right)^2 \cdot \left(\frac{t}{\tau_{t1}}\right)}} + \frac{1-y}{\left(1+\frac{t}{\tau_{t2}}\right)\sqrt{1+\left(\frac{\omega_0}{z_0}\right)^2 \cdot \left(\frac{t}{\tau_{t2}}\right)}}\right] \qquad \text{Eq.3}$$

where $2\omega_0$ and $2z_0$ represent the diameter (lateral focal radius) and height (optical radius) of detection volume, respectively. T is the percentage of molecules in triplet state and τ_t is the triplet relaxation time (or the time particles spend in the triplet state). In Eq.3, N·y and N·(1-y) represent the molecules with diffusion time τ_{t1} and τ_{t2}, respectively.

From the SymPhoTime software, both fractions of the two diffusion species are calculated based on the fitted ρ_1 and ρ_2 values using Eq.4

$$fraction\ 1\ (\%) = \frac{\rho_1}{\rho 1+\rho 2} \times 100\% \qquad \text{Eq.4}$$

To analyze the curves, initially a single-species fit was performed. When the residuals of the fit were not satisfactory, a dual-species fit was performed, with leaving the diffusion of species 1 (D_1) and species 2 (D_2) free. If one of the species has a diffusion coefficient in the range of intact mRNA (between 17 and 22 $\mu m^2 \cdot s^{-1}$), or intact pDNA (between 2.0 and 5.0 $\mu m^2 \cdot s^{-1}$) this fit is considered reliable and the fraction of intact mRNA or pDNA is calculated from Eq.4, with species one being the slow component. For pDNA, this was always the case. When the diffusion coefficient is slower than degraded mRNA (< 300 $\mu m^2 \cdot s^{-1}$) but higher than intact mRNA (> 22 $\mu m^2 \cdot s^{-1}$) (red dots in calibration curve), a second dual-species fit was performed, where the D of the slow component is fixed to 20 $\mu m^2 \cdot s^{-1}$ for mRNA. Again, the fraction of intact mRNA is calculated from Eq.4, with species one being the slow component. As shown in supplementary Figure 2, taking into account the molecular brightness of the species did not lead to improved calibration curves.

Single Particle Tracking (SPT)

In Single Particle Tracking (SPT) one uses fast and sensitive fluorescence microscopy to localize individual mobile fluorescent particles or molecules in time and space[84]. Briefly, the motion of fluorescently labeled mRNA or pDNA is imaged as time-lapse videos by a fast and sensitive electron-multiplying charge-coupled device (EMCCD) camera. Then, for every frame, the center location of fluorescently labeled mRNA or pDNA molecules is determined. Secondly, based on this list with particle coordinates, motion trajectories are created for every movie. For each trajectory a diffusion coefficient is calculated, while from the collection of trajectories also the concentration of particles was calculated according to the method described by Röding *et al.*[85].

All SPT measurements were performed on a swept-field confocal microscope (Nikon LiveScan) attached to a Nikon Eclipse Ti-E inverted microscope (Nikon Instruments Europe B.V., Brussel, Belgium), equipped with an oil immersion lens (100× NA1.4, Nikon, Japan). A solid-state laser of 640 nm was used to excite the fluorophores. Videos of the fluorescent molecules were acquired with the NIS Elements software package (Nikon) using an EMCCD camera (Cascade II:512; Roper Scientific, AZ, USA). A total of 5 µL of sample was mounted on a microscopy slide using an adhesive spacer (Secure-Seal™ spacer, 9 mm diameter, 0.12 mm deep; Molecular Probes, OR, USA) and 30 movies of 3 s with a temporal resolution of 30 ms were recorded at different locations within the sample at about 5 µm above the glass coverslip. The experiment was carried out in triplicate at 22 °C. More than 1000 trajectories were analyzed for each sample.

Statistical analysis

Results are shown as mean ± standard deviation. Experiment were performed at least in triplicate on independent days. Significance between the means of two groups was tested using 2-way ANOVA with the GraphPad Prism software. A P-value < 0.05 was considered to be significant.

Acknowledgements

Heyang Zhang acknowledged the financial support from China Scholarship Council (CSC), and appreciated Dr. Brans for sharing his expertise in the microscopy practice and data analysis. Moreover, Zhang gratefully appreciated Dr. Sauvage, Dr. Peynshaert, Dr. Devoldere, An-Katrien Minnaert and Mike Wels for providing bovine vitreous. Last but not least, the blood donor Dr. Brans, Dr. Lucas, Dr. De Backer, Dr. Rein Verbeke, Dr. Merckx and Roberta Guagliardo, was especially much appreciated. This work was financially supported by Europe Research Council (ERC) under the European Union's Horizon 2020 research and innovation program (grant agreement [648214]) and the Research Foundation-Flanders (research project G006714 N).

Conflict of interest: None.

Reference

[1] J. C. Kaczmarek, P. S. Kowalski, D. G. Anderson, *Genome Med.* **2017**, *9*, 60.

[2] J. N. Jarvis, B. Frank Mark, *Genome Med.* **2010**, *2*, 44.

[3] M. K. Lin, M. J. Farrer, *Genome Med.* **2014**, *6*, 1.

[4] L. Bertram, R. E. Tanzi, *Nat. Rev. Neurosci.* **2008**, *9*, 768.

[5] S. Goodwin, J. D. McPherson, W. R. McCombie, *Nat. Rev. Genet.* **2016**, *17*, 333.

[6] L. Zhu, R. I. Mahato, *Expert Opin. Drug Deliv.* **2010**, *7*, 1209.

[7] U. Lä, E. Wagner, *Chem. Rev.* **2015**, *115*, 11043.

[8] K. Buyens, B. Lucas, K. Raemdonck, K. Braeckmans, J. Vercammen, J. Hendrix, Y. Engelborghs, S. C. De Smedt, N. N. Sanders, *J. Control. Release* **2008**, *126*, 67.

[9] L. M. P. Vermeulen, T. Brans, S. C. De Smedt, K. Remaut, K. Braeckmans, *Nano Today* **2018**, *21*, 74.

[10] M. Fakruddin, K. S. Bin Mannan, A. Chowdhury, R. M. Mazumdar, M. N. Hossain, S. Islam, M. A. Chowdhury, *J. Pharm. Bioallied Sci.* **2013**, *5*, 245.

[11] T. Trcek, H. Sato, R. H. Singer, L. E. Maquat, *Genes Dev.* **2013**, *27*, 541.

[12] D. Lechardeur, K.-J. Sohn, M. Haardt, P. B. Joshi, M. Monck, R. W. Graham, B. Beatty, J. Squire, H. O'brodovich, G. L. Lukacs, *Gene Ther.* **1999**, *6*, 482.

[13] D. Huber, L. Voith von Voithenberg, G. V. Kaigala, *Micro Nano Eng.* **2018**, *1*, 15.

[14] H. H. Chen, Y.-P. Ho, X. Jiang, H.-Q. Mao, T.-H. Wang, K. W. Leong, *Nano Today* **2009**, *4*, 125.

[15] J. L. Kirschman, S. Bhosle, D. Vanover, E. L. Blanchard, K. H. Loomis, C. Zurla, K. Murray, B. C. Lam, P. J. Santangelo, W. H. Coulter, *Nucleic Acids Res.* **2017**, *45*, 290.

[16] K. Remaut, B. Lucas, K. Braeckmans, N. N. Sanders, S. C. De Smedt, J. Demeester, *J. Control. Release* **2005**, *103*, 259.

[17] K. Raemdonck, K. Remaut, B. Lucas, N. N. Sanders, J. Demeester, S. C. De Smedt, *Biochemistry* **2006**, *45*, 10614.

[18] K. Remaut, B. Lucas, K. Braeckmans, N. N. Sanders, J. Demeester, S. C. De Smedt, *Biochemistry* **2006**, *45*, 1755.

[19] K. Remaut, B. Lucas, K. Braeckmans, J. Demeester, S. C. De Smedt, *J. Control. Release* **2006**, *117*, 256.

[20] K. Remaut, N. Symens, B. Lucas, J. Demeester, S. C. De Smedt, *J. Control. Release* **2010**, *144*, 65.

[21] J. A. J. Fitzpatrick, B. F. Lillemeier, *Curr. Opin. Struct. Biol.* **2011**, *21*, 650.

[22] R. Macháň, T. Wohland, *FEBS Lett.* **2014**, *588*, 3571.

[23] P. Heissig, W. Schrimpf, P. Hadwiger, E. Wagner, D. C. Lamb, *PLoS One* **2017**, *12*, 1.

[24] K. Remaut, N. N. Sanders, B. G. De Geest, K. Braeckmans, J. Demeester, S. C. De Smedt, *Mater. Sci. Eng. R Reports* **2007**, *58*, 117.

[25] E. Zagato, K. Forier, T. Martens, K. Neyts, J. Demeester, S. De Smedt, K. Remaut, K. Braeckmans, *Nanomedicine* **2014**, *9*, 913.

[26] K. Braeckmans, K. Buyens, W. Bouquet, C. Vervaet, P. Joye, F. De Vos, L. Plawinski, D. Loı¨c, E. Angles-Cano, N. N. Sanders, J. Demeester, S. C. De Smedt, *Nano Lett.* **2010**, *10*, 4435.

[27] G. R. Dakwar, E. Zagato, J. Delanghe, S. Hobel, A. Aigner, H. Denys, K. Braeckmans, W. Ceelen, S. C. De Smedt, K. Remaut, *Acta Biomater.* **2014**, *10*, 2965.

[28] T. F. Martens, D. Vercauteren, K. Forier, H. Deschout, K. Remaut, R. Paesen, M. Ameloot, J. F. Engbersen, J. Demeester, S. C. De Smedt, K. Braeckmans, *Nanomedicine* **2013**, *8*, 1955.

[29] X. Yang, L. Steukers, K. Forier, R. Xiong, K. Braeckmans, K. Van Reeth, H. Nauwynck, *PLoS One* **2014**, *9*, e11026.

[30] D. Vercauteren, H. Deschout, K. Remaut, J. F. J. Engbersen, A. T. Jones, J. Demeester, S. C. De Smedt, K. Braeckmans, *ACS Nano* **2011**, *5*, 7874.

[31] C. M. Knobler, W. M. Gelbart, A. Gopal, Z. H. Zhou, *RNA* **2012**, *18*, 284.

[32] B. Tinland, H. Ren, C. Desruisseaux, L. C. McCormick, G. Drouin, G. W. Slater, *Electrophoresis* **2001**, *22*, 2424.

[33] K. Braeckmans, K. Buyens, B. Naeye, D. Vercauteren, H. Deschout, K. Raemdonck, K. Remaut, N. N. Sanders, J. Demeester, S. C. De Smedt, *J. Control. Release* **2010**, *148*, 69.

[34] M. . Paridah, A. Moradbak, A. . Mohamed, F. abdulwahab taiwo Owolabi, M. Asniza, S. H. . Abdul Khalid, in *Gene Ther. Challenges*, **2015**, pp. 145–177.

[35] J. Devoldere, K. Peynshaert, H. Dewitte, C. Vanhove, L. De Groef, L. Moons, S. Y. Özcan, D. Dalkara, S. C. De Smedt, K. Remaut, *J. Control. Release* **2019**, *307*, 315.

[36] M. Shariati, H. Zhang, L. Van De Sande, B. Descamps, C. Vanhove, W. Willaert, W. Ceelen, S. C. De Smedt, K. Remaut, *Pharm. Res.* **2019**, *36*, 126.

[37] S. L. Mendelsohn, D. A. Young, *BBA Sect. Nucleic Acids Protein Synth.* **1978**, *519*, 461.

[38] C. Gaillard, F. Strauss, *Tech. Tips Online* **1998**, *3*, 63.

[39] TA-Hsiu Liao, *J. Biol. Chem.* **1975**, *250*, 3831.

[40] H. Zhang, S. C. De Smedt, K. Remaut, *Acta Biomater.* **2018**, *75*, 358.

[41] J. Gadi, A. E. Kalyani, R. Ae, K.-A. Kong, A. E. Hyoung, W. Park, A. E. Myoung, H. Kim, *Mol Biotechnol*

2009, *42*, 41.

[42] C. Rosazza, H. Deschout, A. Buntz, K. Braeckmans, M.-P. Rols, A. Zumbusch, *Mol. Ther. - Nucleic Acids* **2016**, *5*, e286.

[43] U. Sahin, K. Karikó, Ö. Türeci, *Nat. Rev. Drug Discov.* **2014**, *13*, 759.

[44] K. A. Hajj, K. A. Whitehead, *Nat. Rev. Mater.* **2017**, *2*, 17056.

[45] M. Rarbach, U. Kettling, A. Koltermann, M. Eigen, *Methods* **2001**, *24*, 104.

[46] J. L. Weickmann+, D. G. Glitz, J. J. Beintema, P. Wietzes, J. L. Weickmann, D. G. Glitz, *J. Biol. Chem.* **1982**, *257*, 8705.

[47] F. Acquati, M. Lualdi, S. Bertilaccio, L. Monti, G. Turconi, M. Fabbri, A. Grimaldi, A. Anselmo, A. Inforzato, A. Collotta, L. Cimetti, C. Riva, L. Gribaldo, P. Ghia, R. Taramelli, G. Klein, *PANS* **2013**, *110*, 8140.

[48] N. Potenza, V. Salvatore, A. Migliozzi, V. Martone, V. Nobile, A. Russo, *Nucleic Acids Res* **2006**, *34*, 2906.

[49] J. B. P. Landré, P. W. Hewett, J. M. Olivot, P. Friedl, Y. Ko, A. Sachinidis, M. Moenner, *J. Cell. Biochem.* **2002**, *86*, 540.

[50] C. H. Jones, C.-K. Chen, A. Ravikrishnan, S. Rane, B. A. Pfeifer, *Mol. Pharm.* **2013**, *10*, 4082.

[51] K. Remaut, N. N. Sanders, F. Fayazpour, J. Demeester, S. C. De Smedt, *J. Control. Release* **2006**, *115*, 335.

[52] G. L. Lukacs, P. Haggie, O. Seksek, D. Lechardeur, N. Freedman, A. S. Verkman, *J. Biol. Chem.* **2000**, *275*, 1625.

[53] S. Ivanchenko, D. C. Lamb, *Supramol. Struct. Funct. 10* **2011**, 1.

[54] Y. H. Foo, N. Naredi-Rainer, D. C. Lamb, S. Ahmed, T. Wohland, *Biophys. J.* **2012**, *102*, 1174.

[55] M. Tsoi, T. T. Do, V. Tang, J. A. Aguilera, C. C. Perry, J. R. Milligan, *Biophys. Chem.* **2010**, *147*, 104.

[56] F. Ke, Y. K. Luu, M. Hadjiargyrou, D. Liang, *PLoS One* **2010**, *5*, 13308.

[57] C. M. Wiethoff, C. R. Middaugh, *Methods Mol. Biol.* **2014**, *65*, 349.

[58] R. M. Robertson, S. Laib, D. E. Smith, *Diffusion of Isolated DNA Molecules: Dependence on Length and Topology*, **2006**.

[59] Q. Wang, Y. Chen, L. Wang, X. Zhang, H. Huang, W. Teng, *Int. J. Nanomedicine* **2015**, *10*, 597.

[60] K. Kawabata, Y. Takakura, M. Hashida, *Pharm. Res.* **1995**, *12*, 825.

[61] W. Yao, C. Mei, X. Nan, L. Hui, *Gene* **2016**, *590*, 142.

[62] C. Yu, M. Hsu, H. Uludağ, *BMC Biotechnol.* **2008**, *8*, 23.

[63] K. Zagorovsky, L. Y. T. Chou, W. C. W. Chan, *PANS* **2016**, *113*, 13600.

[64] L. Pitkä, M. Ruponen, J. Nieminen, A. Urtti, *Pharm. Res.* **2003**, *20*, 576.

[65] L. Peeters, N. N. Sanders, K. Braeckmans, K. Boussery, J. Van De Voorde, S. C. De Smedt, J. Demeester, *Investig. Ophthalmol. Vis. Sci.* **2005**, *46*, 3553.

[66] G. Bajaj, Y. Yeo, *Pharm. Res.* **2010**, *27*, 735.

[67] C. M. Wiethoff, C. R. Middaugh, *J. Pharm. Sci.* **2003**, *92*, 203.

[68] Y. Fujiwara, H. Kikuchi, S. Aizawa, A. Furuta, Y. Hatanaka, C. Konya, K. Uchida, K. Wada, T. Kabuta, *Autophagy* **2013**, *9*, 1167.

[69] A. Siwaszek, M. Ukleja, A. Dziembowski, *RNA Biol.* **2014**, *11*, 1122.

[70] A. Wittrup, A. Ai, X. Liu, P. Hamar, R. Trifonova, K. Charisse, M. Manoharan, T. Kirchhausen, J. Lieberman, *Nat. Biotechnol.* **2015**, *33*, 870.

[71] R. Wattiaux, N. Laurent, S. Wattiaux-De Coninck, M. Jadot, *Adv. Drug Deliv. Rev.* **2000**, *41*, 201.

[72] T. E. ; Tjelle, A. Brech, L. K. Juvet, G. Griffiths, T. Berg, *J. Cell Sci.* **1996**, *109*, 2905.

[73] H. Schulze, T. Kolter, K. Sandhoff, *BBA - Mol. Cell Res.* **2008**, *1793*, 674.

[74] Y. Fujiwara, K. Wada, T. Kabuta, *J. Biochem* **2017**, *161*, 145.

[75] Rajashree A. Deshpande, Vepatu Shankar, *Crit. Rev. Microbiol.* **2002**, *28*, 79.

[76] C. J. Evans, R. J. Aguilera, *Gene* **2003**, *322*, 1.

[77] C. Leonhardt, G. Schwake, T. R. Stögbauer, S. Rappl, J.-T. Kuhr, T. S. Ligon, J. O. Rädler, *Nanomedicine Nanotechnology, Biol. Med.* **2014**, *10*, 679.

[78] K. A. Dickson, M. C. Haigis, R. T. Raines, *Prog. Nucleic Acid Res. Mol. Biol.* **2005**, *80*, 349.

[79] K. Remaut, B. Lucas, K. Braeckmans, N. N. Sanders, J. Demeester, S. C. De Smedt, *Biomacromolecules* **2007**, *8*, 1333.

[80] A. Sasaki, M. Kinjo, *J. Control. Release* **2010**, *143*, 104.

[81] K. Rombouts, K. Braeckmans, K. Remaut, *Bioconjugate Chem.* **2016**, *27*, 280.

[82] K. Rombouts, T. F. Martens, E. Zagato, J. Demeester, S. C. De Smedt, K. Braeckmans, K. Remaut, *Mol. Pharm.* **2014**, *11*, 1359.

[83] K. Braeckmans, B. G. Stubbe, K. Remaut, J. Demeester, S. C. De Smedt, *J. Biomed. Opt.* **2006**, *11*, 044013.

[84] K. Braeckmans, D. Vercauteren, J. Demeester, S. C. De Smedt, *Nat. Nanotechnol.* **2011**, *6*, 615.

[85] M. Röding, H. Deschout, K. Braeckmans, M. Rudemo, *J. Microsc.* **2013**, *251*, 19.

Graphical abstract

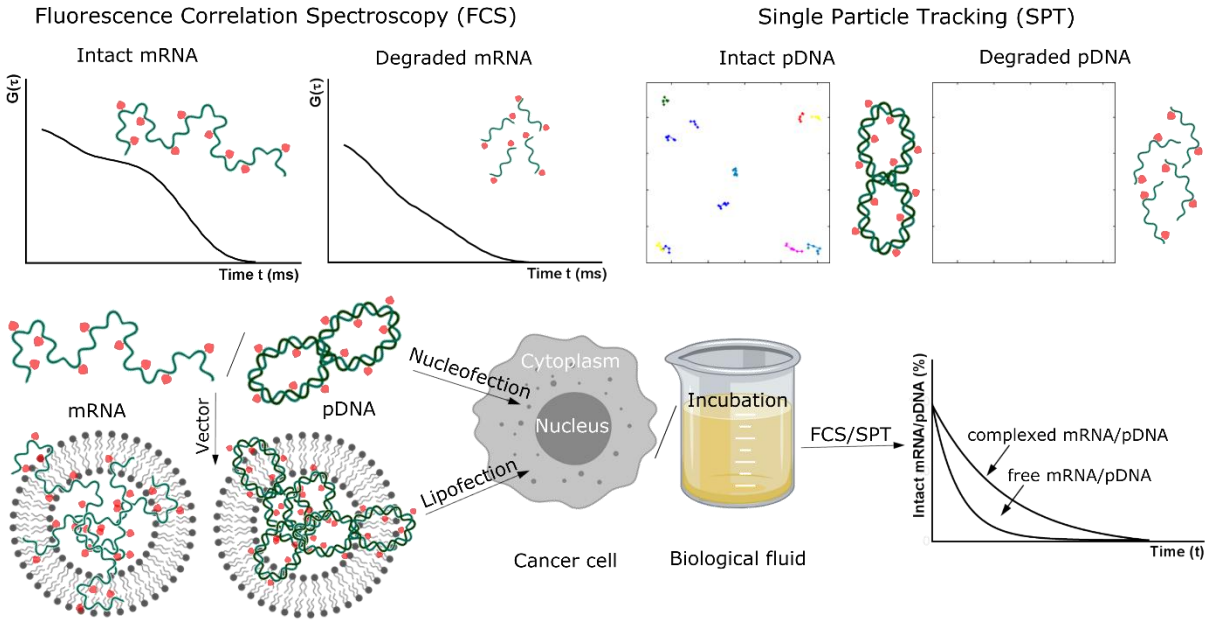

Figures and legends

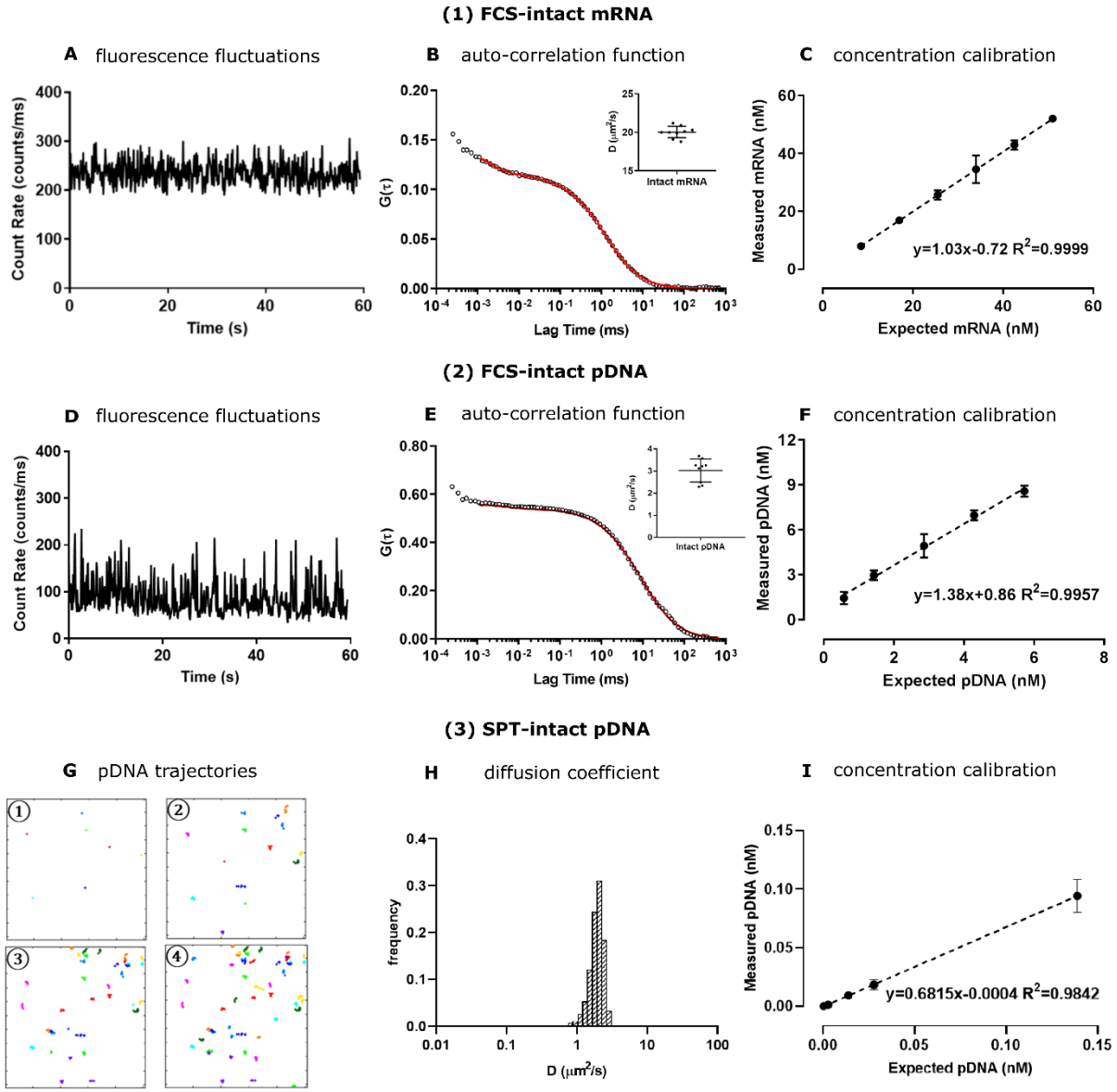

Figure 1. Quantification of (1) Cy5 mRNA and (2, 3) Cy5 pDNA in HEPES buffer. (A) Representative fluorescence fluctuations as a function of time and (B) auto-correlation function G(τ) as a function of lag time during FCS measurements of 6 $\mu g \cdot mL^{-1}$ Cy5 mRNA. (C) Cy5 mRNA was quantified by FCS and auto-correlation analysis within the range of 3-18 $\mu g \cdot mL^{-1}$, where X and Y-axis represent the expected (nM) and measured (nM) concentration of mRNA, respectively. (D) Representative fluorescence fluctuations as a function of time and (E) auto-correlation function G(τ) as a function of lag time during FCS measurements of 5 $\mu g \cdot mL^{-1}$ Cy5 pDNA. (F) Cy5 pDNA was quantified by FCS and auto-correlation analysis within the range of 2-20 $\mu g \cdot mL^{-1}$, where X and Y-axis represent

the expected (nM) and measured (nM) concentration of pDNA, respectively. (G) Individual trajectories and representative movie of Cy5 pDNA (0.05 μg·mL^{-1}) motion in HEPES buffer. By using an in house-developed program, (H) the diffusion coefficient of Cy5 pDNA and (I) the concentration calibration within the range of 0.001-0.5 μg·mL^{-1} of pDNA was quantified, where the X and Y-axis represented the expected (nM) and measured (nM) concentration of pDNA respectively. All the experiments were performed for three independent times.

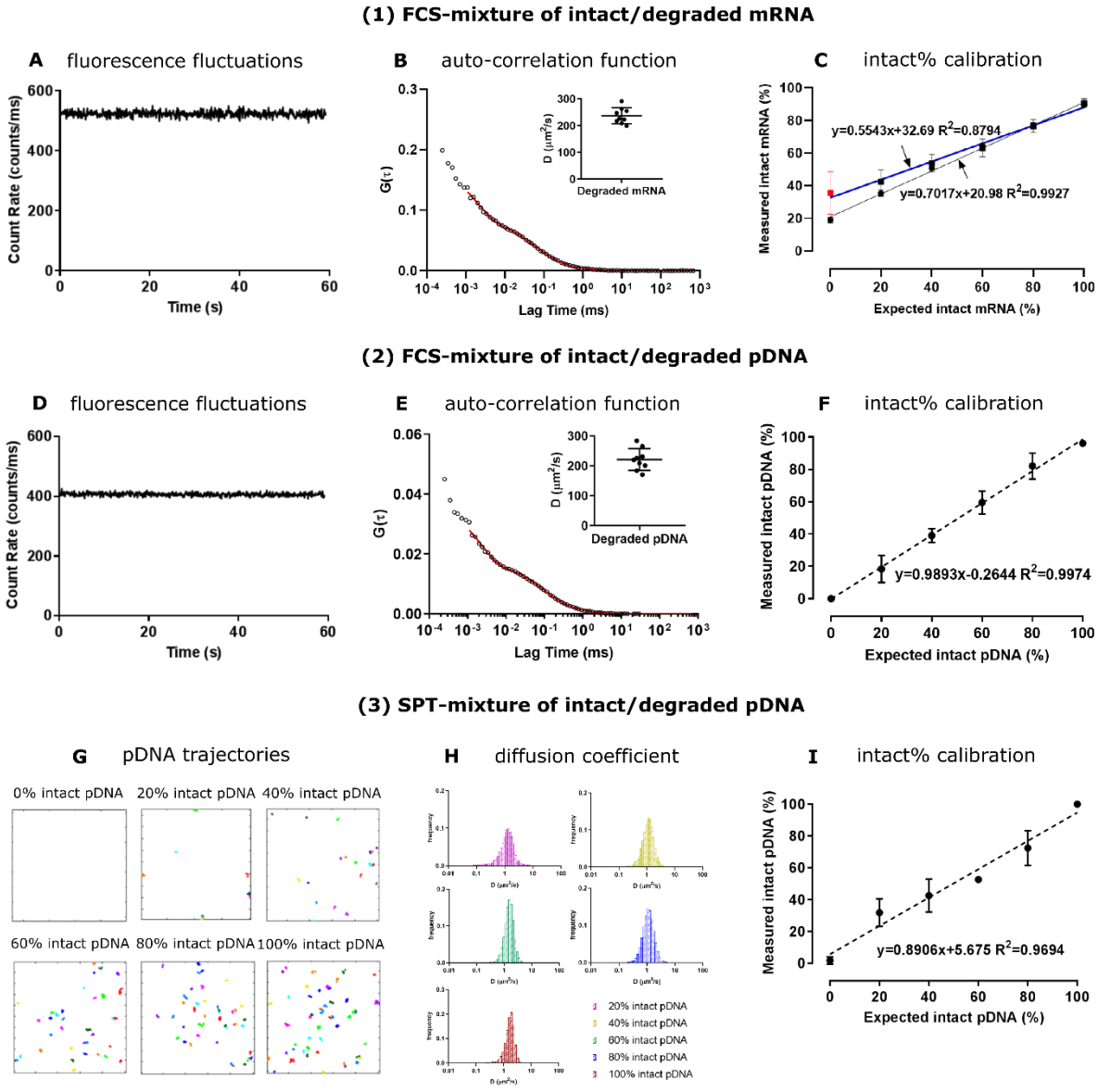

Figure 2. Quantification of (1) Cy5 mRNA and (2, 3) Cy5 pDNA in intact/degraded mixture with known w/w ratios of 0/100, 20/80, 40/60, 60/40, 80/20 and 100/0 %. (A) Representative fluorescence fluctuations over time and (B) auto-correlation function as a function of lag time during FCS measurements of fully degraded mRNA in HEPES buffer. (C) Fraction of intact Cy5 mRNA was quantified by dual-species auto-correlation analysis either by leaving

both components free (blue line) or by fixing the diffusion coefficient of the slow component to 20 $\mu m^2 \cdot s^{-1}$ (black line). Red data points indicate the analysis where the dual-species fit generated a slow component with a diffusion coefficient that did not correspond to intact mRNA. (D) Representative fluorescence fluctuations over time and (E) auto-correlation function as a function of lag time during FCS measurements of fully degraded pDNA in HEPES buffer. (F) Fraction of intact pDNA was quantified by dual-species auto-correlation analysis, where diffusion of both components was left free. (G) Individual trajectories of intact/degraded Cy5 pDNA mixture. (H) Distribution of diffusion coefficient of pDNA in the mixtures of intact/degraded pDNA. (I) Fraction of intact pDNA (%) in the mixture of intact/degraded Cy5 pDNA as quantified by SPT. All the experiments were performed for three independent times.

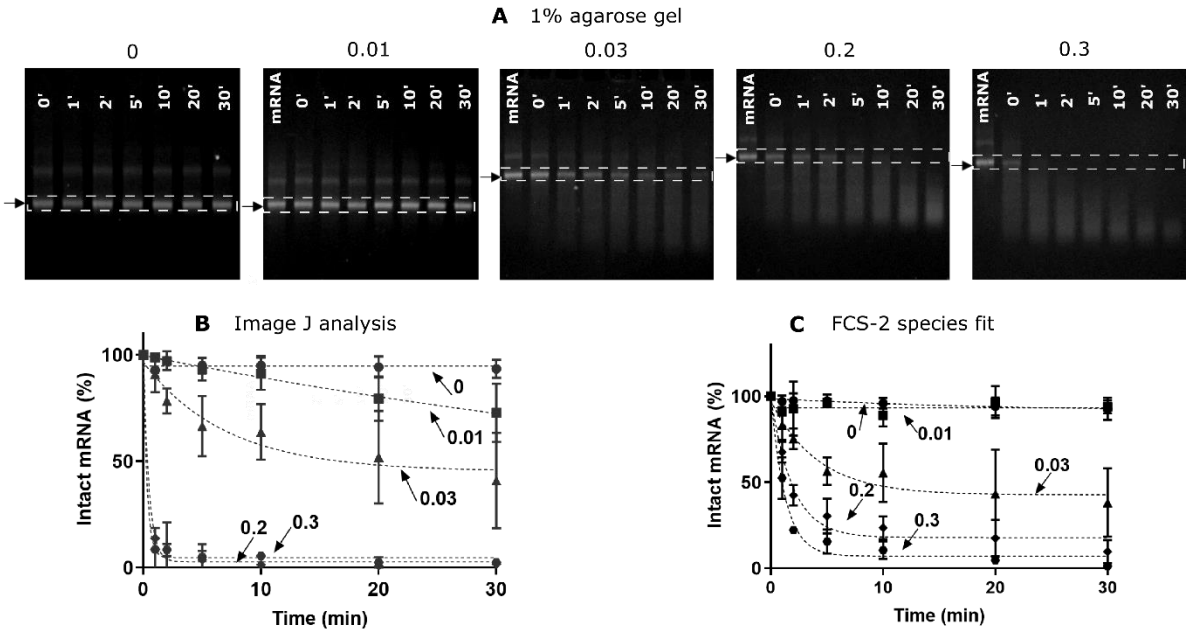

Figure 3. Cy5 mRNA degradation mediated by RNase A and quantified by 1% agarose gel electrophoresis and FCS. (A) Representative gel for mRNA decay by varying amount of RNase A (as showed above the images, Unit per 1 µg mRNA) at 37 °C for 0, 1, 2, 5, 10, 20 and 30 min, as depicted above the lanes. The level of intact mRNA is indicated by the arrow and the white squares. (B) mRNA decay kinetics over time by gel electrophoresis and analyzed by Image J, with different amount of RNase A: 0 $U \cdot \mu g^{-1}$ (circle), 0.01 $U \cdot \mu g^{-1}$ (square), 0.03 $U \cdot \mu g^{-1}$ (triangle), 0.2 $U \cdot \mu g^{-1}$ (diamond), 0.3 $U \cdot \mu g^{-1}$ (hexagon). (C) mRNA decay as a function of time with varying amount of RNase A, 0 $U \cdot \mu g^{-1}$ (circle), 0.01 $U \cdot \mu g^{-1}$ (square), 0.03 $U \cdot \mu g^{-1}$ (triangle), 0.2 $U \cdot \mu g^{-1}$ (diamond), 0.3 $U \cdot \mu g^{-1}$ (hexagon),

measured by FCS and dual-species auto-correlation analysis. All experiments were performed for three independent times. Decay parameters are listed in supplementary Table 1 and 2.

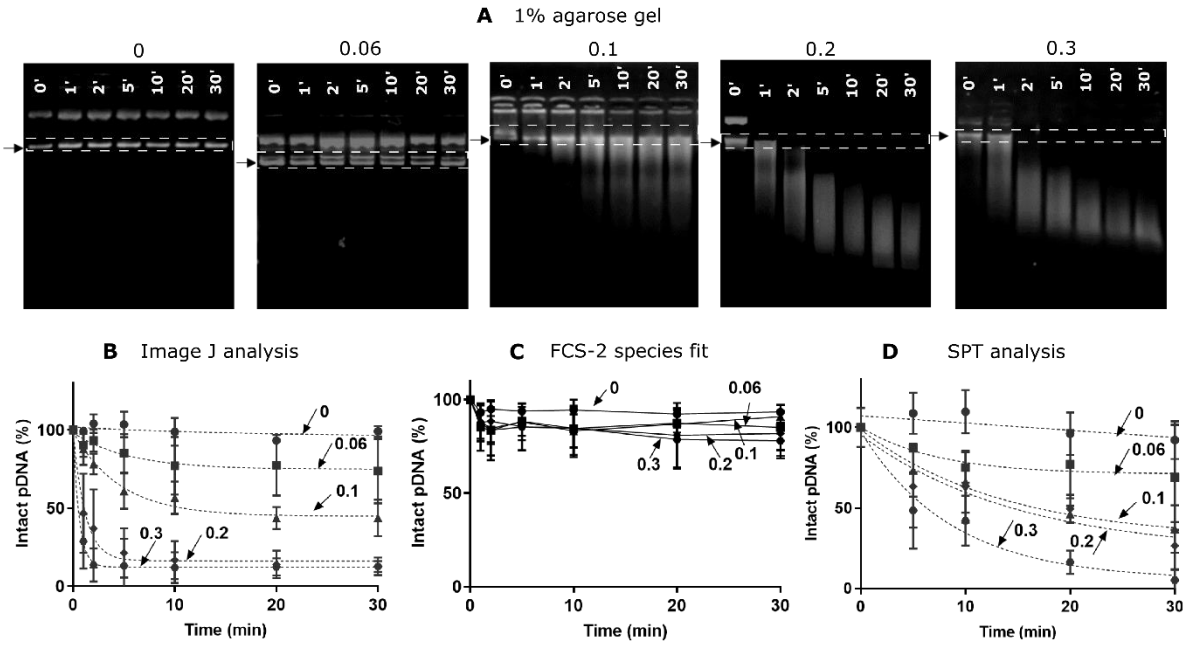

Figure 4. Cy5 pDNA degradation mediated by DNase I and quantified by 1% agarose gel electrophoresis, FCS and SPT. (A) Representative gel for pDNA decay by varying amount of DNase I (as showed above the images) at 37 °C for 0, 1, 2, 5, 10, 20 and 30 min, as depicted above the lanes. The level of intact supercoiled pDNA is indicated by the arrow and the white squares. Quantification of pDNA decay kinetics over time by gel electrophoresis and analyzed by (B) Image J, (C) FCS and (D) SPT, with different amount of DNase I: 0 U·μg^{-1} (circle), 0.06 U·μg^{-1} (square), 0.1 U·μg^{-1} (triangle), 0.2 U·μg^{-1} (diamond), 0.3 U·μg^{-1} (hexagon). All experiments were performed for three independent times. Decay parameters are listed in supplementary Table 3 and 4.

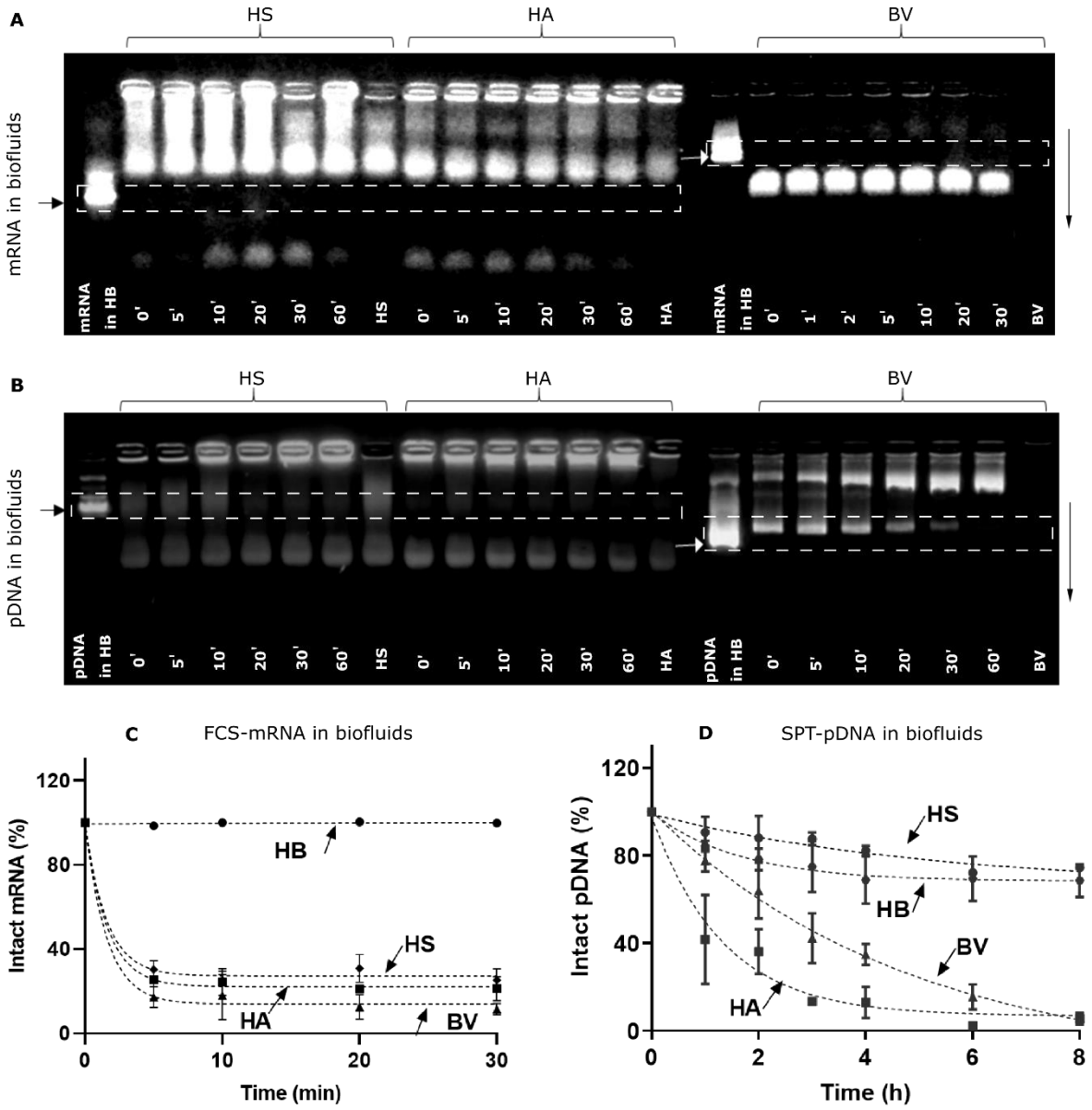

Figure 5. (A-B) Representative gel of mRNA (A) and pDNA (B) degradation in HEPES buffer (HB, as control), human serum (HS), human ascites (HA) and bovine vitreous (BV) as a function of time at 37 °C. The arrow and white squares indicate the level of intact mRNA and supercoiled pDNA, respectively. (C) Quantification of mRNA decay in HB (circle), HS (diamond), HA (square) and BV (triangle) at 37 °C for 0, 5, 10, 20, 30 min as determined by FCS. (D) Quantification of Cy5 pDNA degradation in HB (circle), HS (diamond), HA (square) and BV (triangle) at 37 °C for 0, 1, 2, 3, 4, 6 and 8 h as determined by SPT. All experiments were performed for three independent times. Decay parameters are listed in supplementary Table 5 and 6.

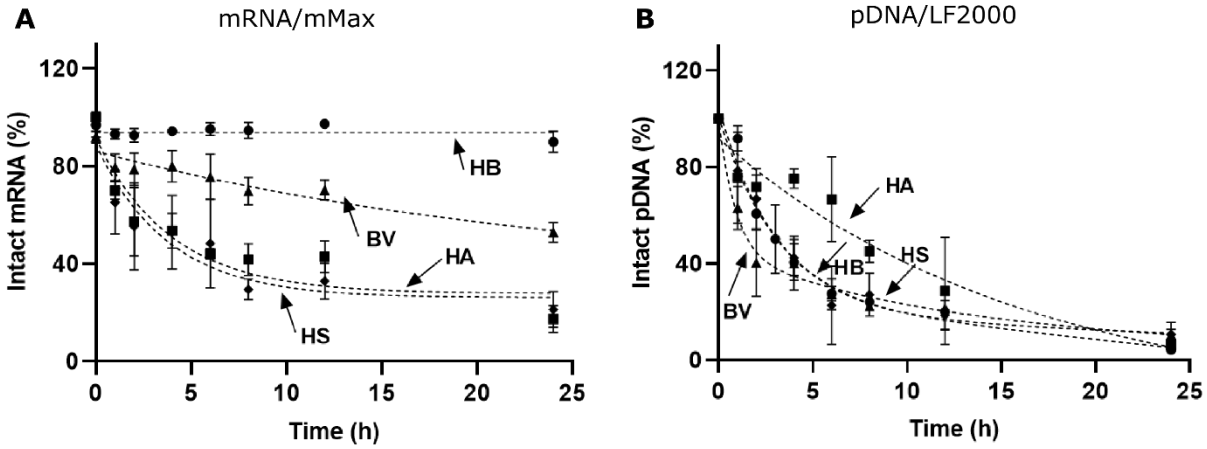

Figure 6. Carrier mediated protection of mRNA and pDNA in biological samples. A stock solution of complexes were incubated in the HB (circle), HS (diamond), HA (square) and BV (triangle) and at the chosen time points, a small aliquot was removed and SDS was added with a final concentration of 3% and incubated at room temperature for 20 min before performing (A) FCS measurements for mRNA and (B) SPT analysis for pDNA, respectively. All the experiments were performed for three independent times. Decay parameters are listed in supplementary Table 5 and 6.

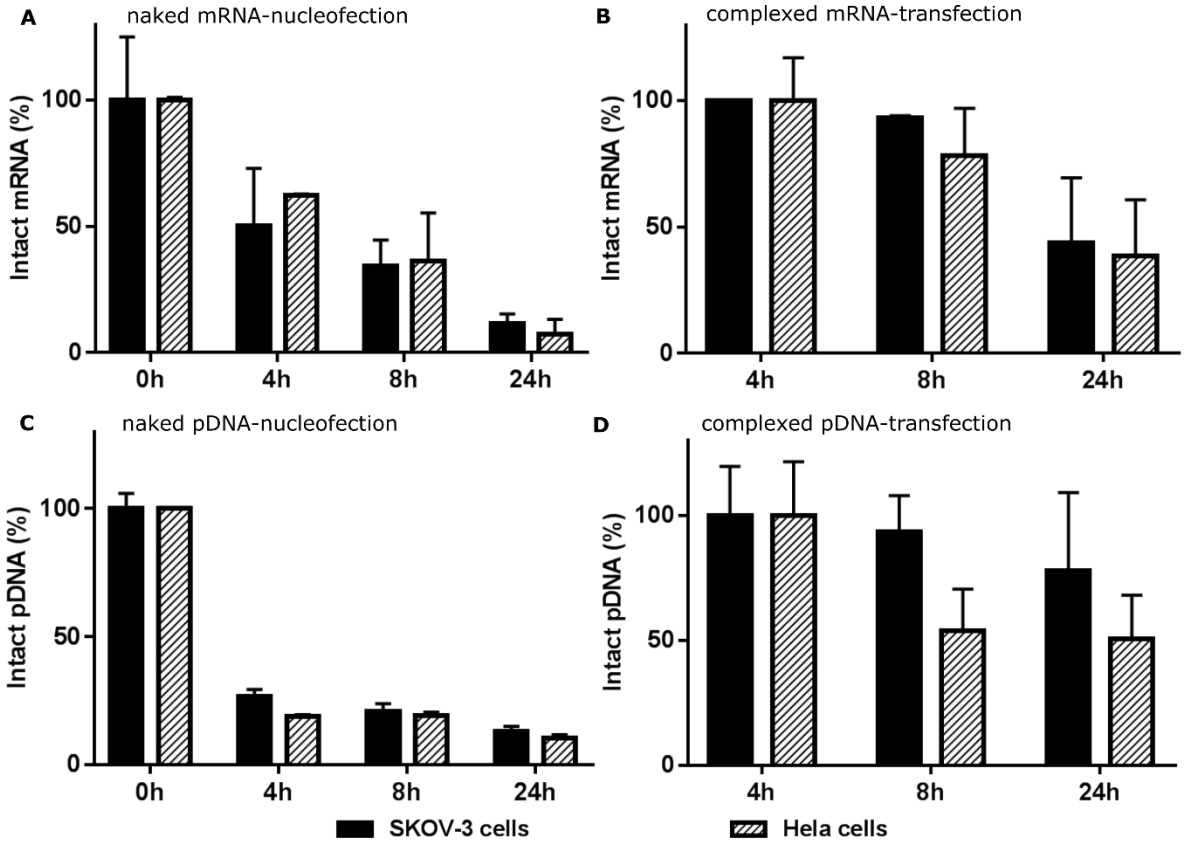

Figure 7. Intracellular degradation of mRNA (A, B) and pDNA (C, D) delivered in naked form by (A, C) nucleofection and (B, D) complexed form by mMax (v/w ratio of 3) and LF2000 respectively in SKOV-3 cells (black bar) and Hela cells (striped bar) At the end of incubation, mRNA or pDNA treated cells were lysed and SDS was then added to the cell lysate to inhibit nuclease activity and release complexed mRNA or pDNA before performing measurements. All the experiments were performed for three independent times.

Supporting information

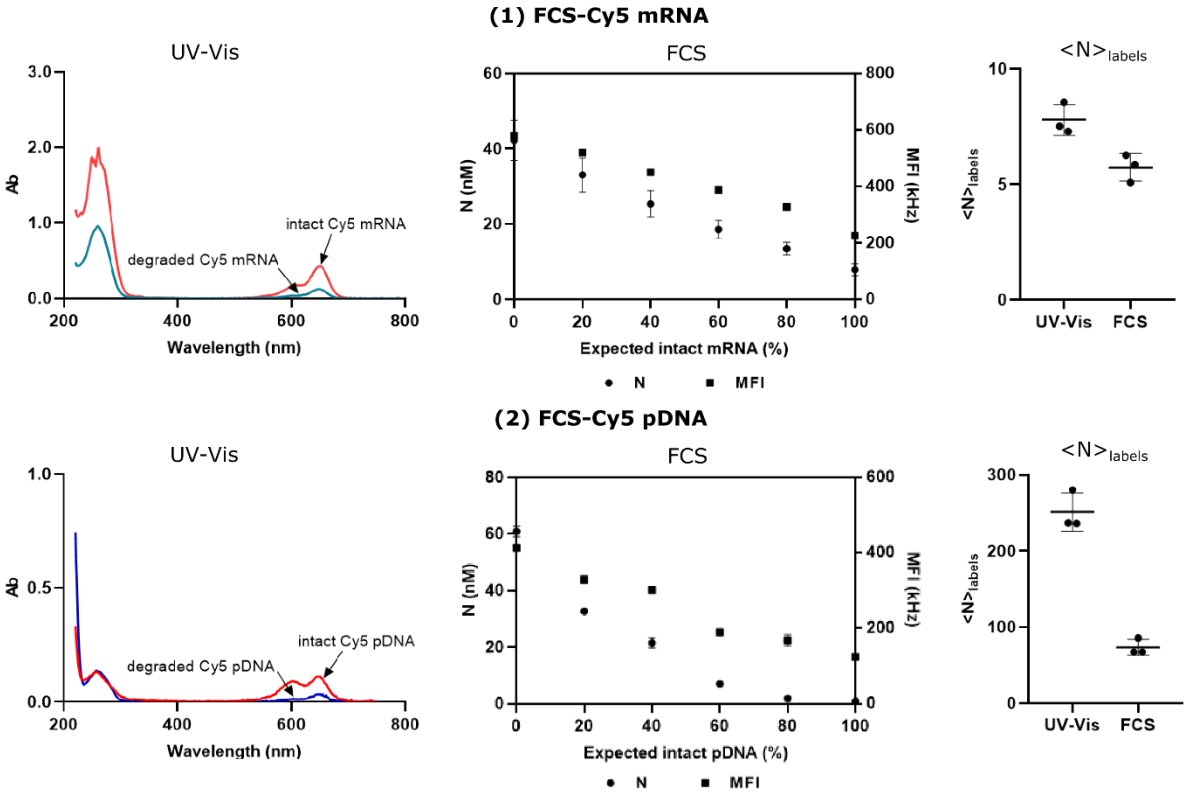

Figure S1. Labeling efficiency of (1) Cy5 mRNA and (2) Cy5 pDNA determined by UV-Vis absorption spectra and FCS. Absorption spectra of intact Cy5 mRNA (or Cy5 pDNA) was measured by Nanodrop 2000 to obtain the concentration of Cy5 (A649) and mRNA or pDNA (A260), from which the labeling efficiency ($<N>_{labels}$) was obtained. By using FCS to quantify the labeling efficiency, the concentration of intact Cy5 mRNA (or Cy5 pDNA) and fully degraded Cy5 mRNA (or Cy5 pDNA) was obtained by FCS fitting (Triplet-state model, dual-species). The labeling efficiency was calculated by dividing $<N>_{degraded}$ by $<N>_{intact}$. All the experiments were performed for three independent times.

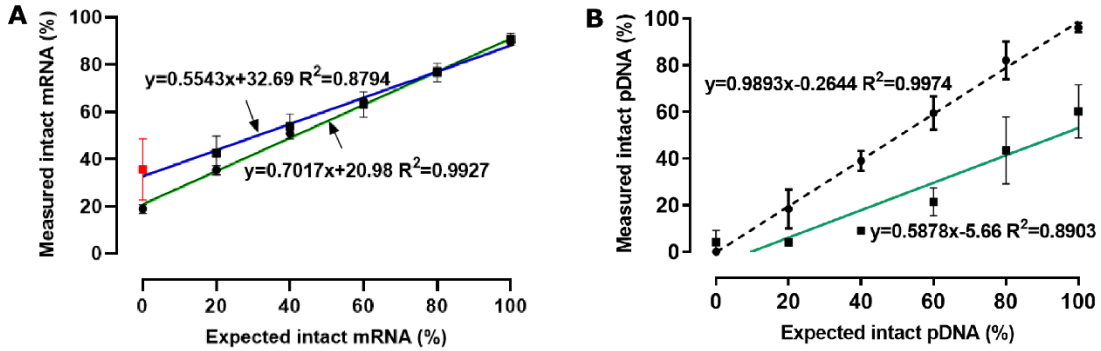

Figure S2. (A) Fraction of intact Cy5 mRNA was quantified by dual-species auto-correlation analysis either by leaving both components free (blue line) or by fixing the diffusion coefficient of the slow component to 20 $\mu m^2 \cdot s^{-1}$ (black line). The calibration curve corrected for molecular brightness is indicated in green. For mRNA, the black and green line overlap. Red data points indicate the analysis where the dual-species fit generated a slow component with a diffusion coefficient that did not correspond to intact mRNA. (B) Fraction of intact pDNA was quantified by dual-species auto-correlation analysis, where diffusion of both components was left free (black dish line) and molecular brightness was taken into account (green line), respectively. To correct for molecular brightness, Eq.4 was replaced by the following equation:

$$fraction\ 1\ (\%) = \frac{\rho_1}{\rho_1 + < N >_{labels} \cdot \Delta QY^2 \cdot \rho_2} \times 100\%$$

where ΔQY represents the changes of quantum yield from component 1 (i.e. intact nucleic acid) to component 2 (i.e. degraded fragments), $<N>_{labels}$ represents the average number of fluorophore per intact nucleic acid molecules. For our experiments, N = 6 ± 1 for mRNA and 73 ± 11 for pDNA and ΔQY = 0.41 ± 0.04 for mRNA and 0.30 ± 0.01 for pDNA, respectively.

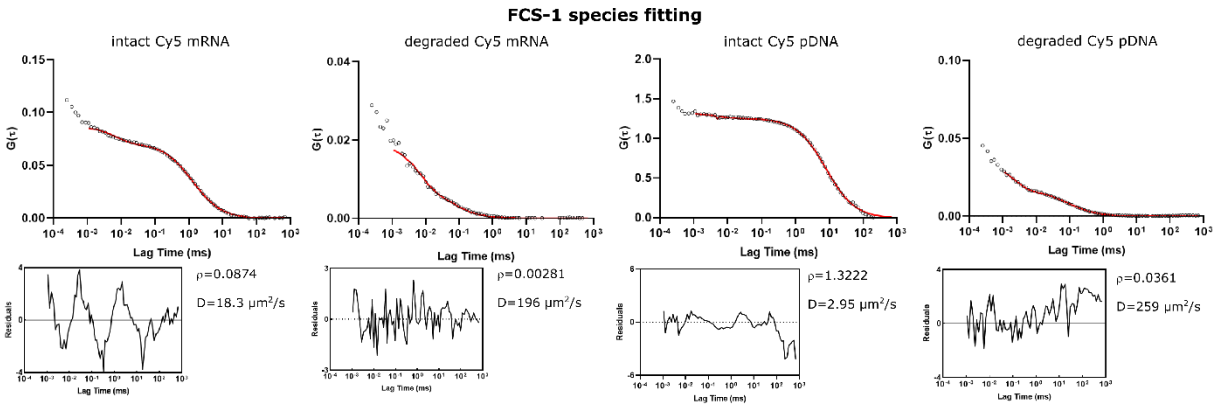

Figure S3. Representative auto-correlation function in function of lag time (open circle) and auto-correlation fitting (Triplet-state, single-species) curve (red line) of intact and degraded Cy5 mRNA (or pDNA) obtained from FCS measurements.

FCS-2 species fitting

(1) FCS-intact/degraded mRNA

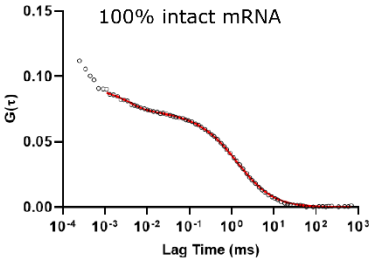

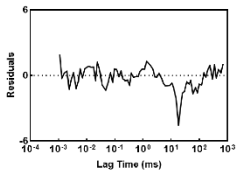

ρ_1=0.08441
D_1=17.5 μm²/s
ρ_2=0.00783
D_2=360 μm²/s
intact %: 92%

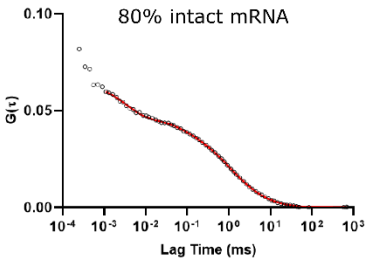

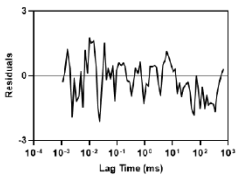

ρ_1=0.04812
D_1=17.0 μm²/s
ρ_2=0.01647
D_2=215 μm²/s
intact %: 75%

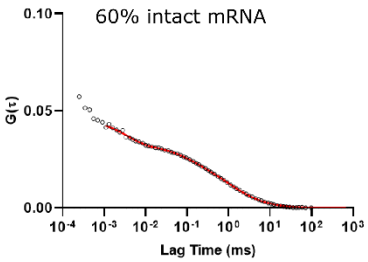

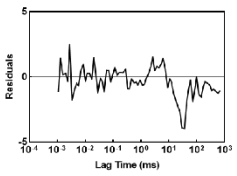

ρ_1=0.02859
D_1=17.7 μm²/s
ρ_2=0.01733
D_2=205 μm²/s
intact %: 62%

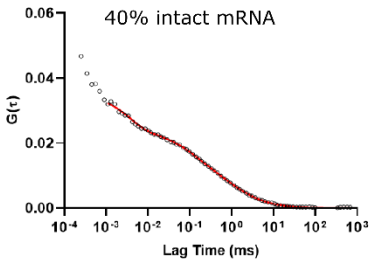

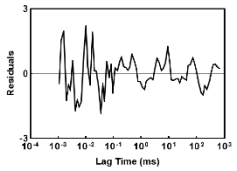

ρ_1=0.01707
D_1=18.1 μm²/s
ρ_2=0.01838
D_2=202 μm²/s
intact %: 48%

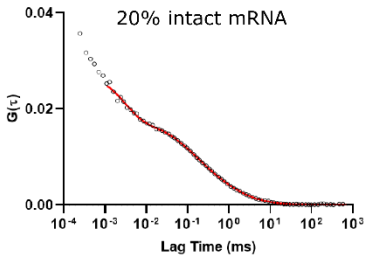

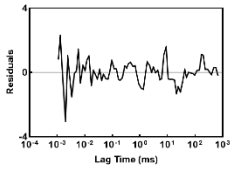

ρ_1=0.00891
D_1=19.2 μm²/s
ρ_2=0.01921
D_2=187 μm²/s
intact %: 31%

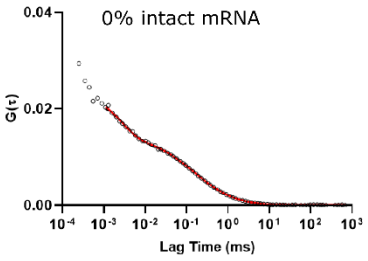

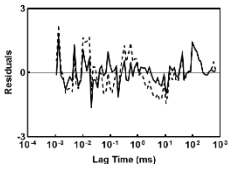

ρ_1=0.01137
D_1=63 μm²/s
ρ_2=0.01327
D_2=322 μm²/s
intact %: 46%

ρ_1=0.00243 D_1=20 μm²/s
ρ_2=0.02024 D_2=166 μm²/s intact %: 10%

(2) FCS-intact/degraded pDNA

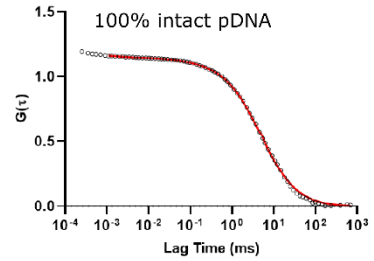

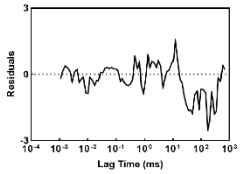

ρ_1=1.1344
D_1=4.73 μm²/s
ρ_2=0.0418
D_2=207 μm²/s
intact %: 96%

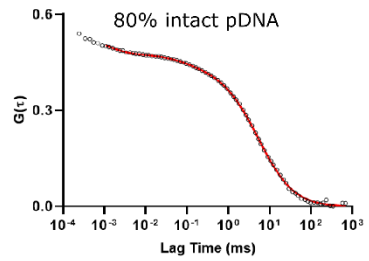

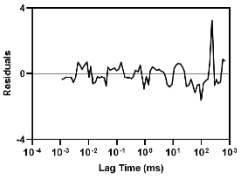

ρ_1=0.4774
D_1=4.39 μm²/s
ρ_2=0.0567
D_2=224 μm²/s
intact %: 89%

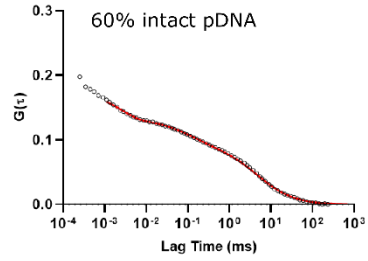

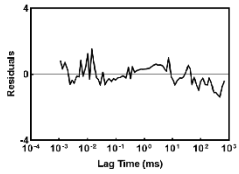

ρ_1=0.1139
D_1=4.44 μm²/s
ρ_2=0.0601
D_2=302 μm²/s
intact %: 65%

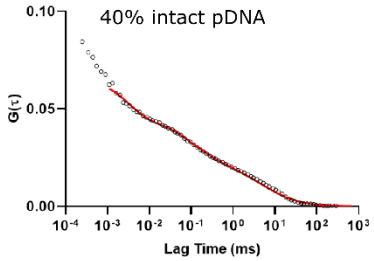

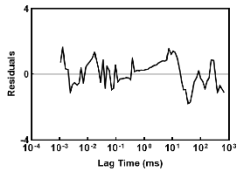

ρ_1=0.0299
D_1=4.16 μm²/s
ρ_2=0.0367
D_2=230 μm²/s
intact %: 44%

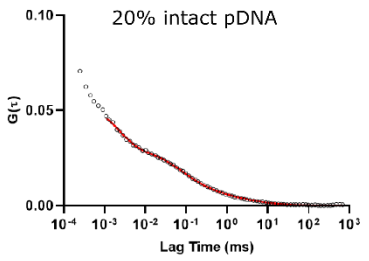

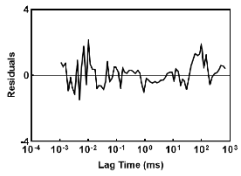

ρ_1=0.00972
D_1=4.4 μm²/s
ρ_2=0.04527
D_2=284 μm²/s
intact %: 17%

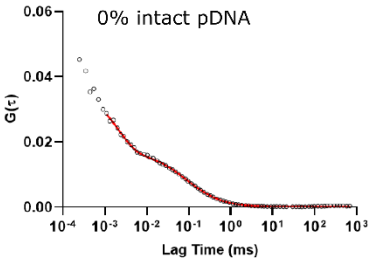

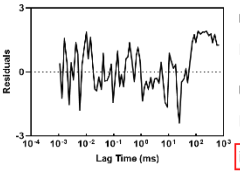

ρ_1=0.00013
D_1=0 μm²/s
ρ_2=0.0366
D_2=269 μm²/s
intact %: 0.4%

Figure S4. Representative auto-correlation function in function of lag time (open circle) and auto-correlation fitting curve (Triplet-state, dual-species, left D_1 and D_2 free; red line) of intact and degraded Cy5 mRNA (or Cy5 pDNA) obtained from FCS measurements. For the 'fully degraded' mRNA, the auto-correlation analysis was performed with dual-species and fixed D_1 of 20 $\mu m^2 \cdot s^{-1}$.

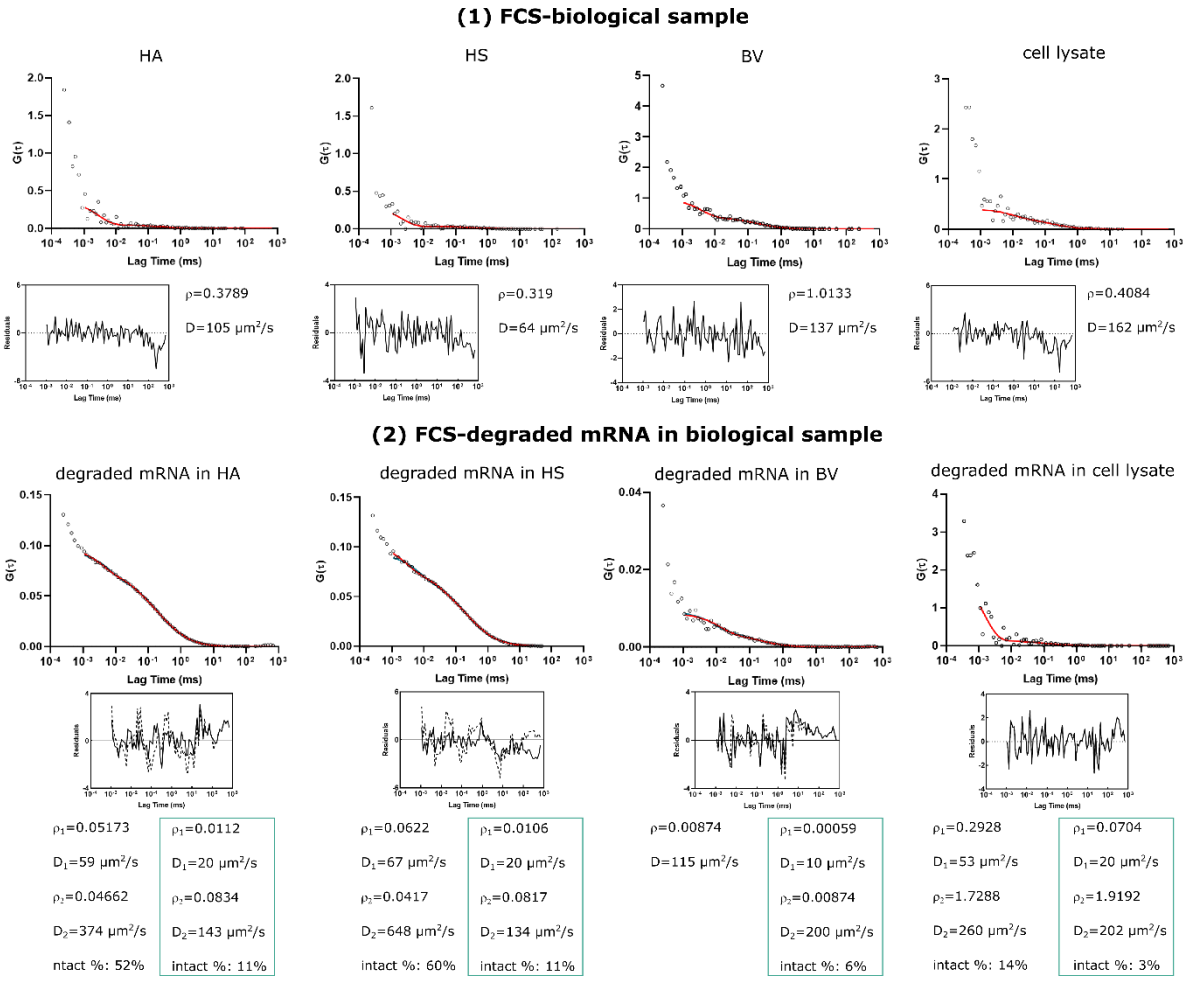

Figure S5. Representative auto-correlation function in function of lag time (open circle) and auto-correlation analysis during FCS measurements of (1) human ascites (HA), human serum (HS), bovine vitreous (BV) and SKOV-3 cell lysate as well as (2) (RNase A-mediated) fully degraded Cy5 mRNA in HA, HS, BV and SKOV-3 cell lysate. The data was fitted using Triplet-state mode with dual-species with D_1 and D_2 free (red line, black line for residuals) and dual-species with fixed D_1 of component 1 of 20 $\mu m^2 \cdot s^{-1}$ (green line, dash line in residuals).

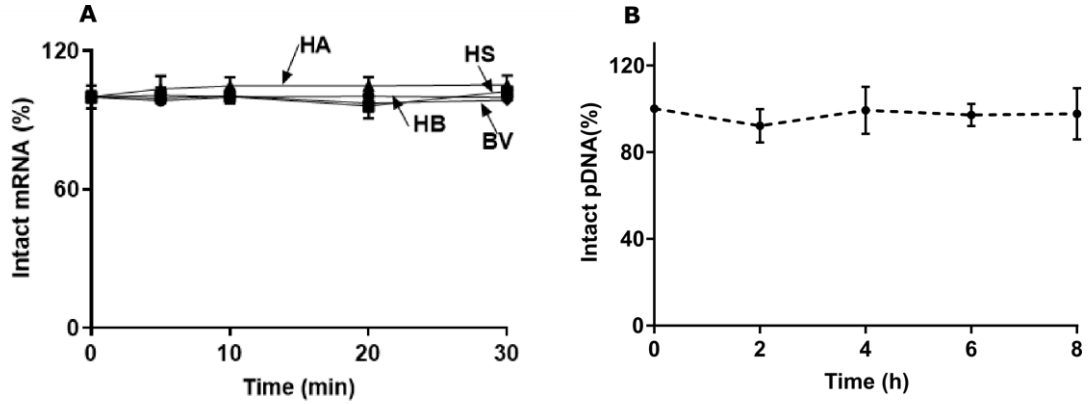

Figure S6. (A) SDS inhibit mRNA degradation in HEPES buffer (HB, control), human ascites (HA, 3% SDS), human serum (HS, 3% SDS) and bovine vitreous (BV, 0.5% SDS), measured by FCS. (B) SDS prevents pDNA from sticking on the polypropylene eppendorf tube when incubated in HEPES buffer. SDS (with final concentration of 3%) was incubated with pDNA in HEPES buffer at 37ºC for 0, 2, 4, 6 and 8 h. At the end of incubation, 5 µL sample was transferred for SPT measurements. All the experiments were performed for three independent times.

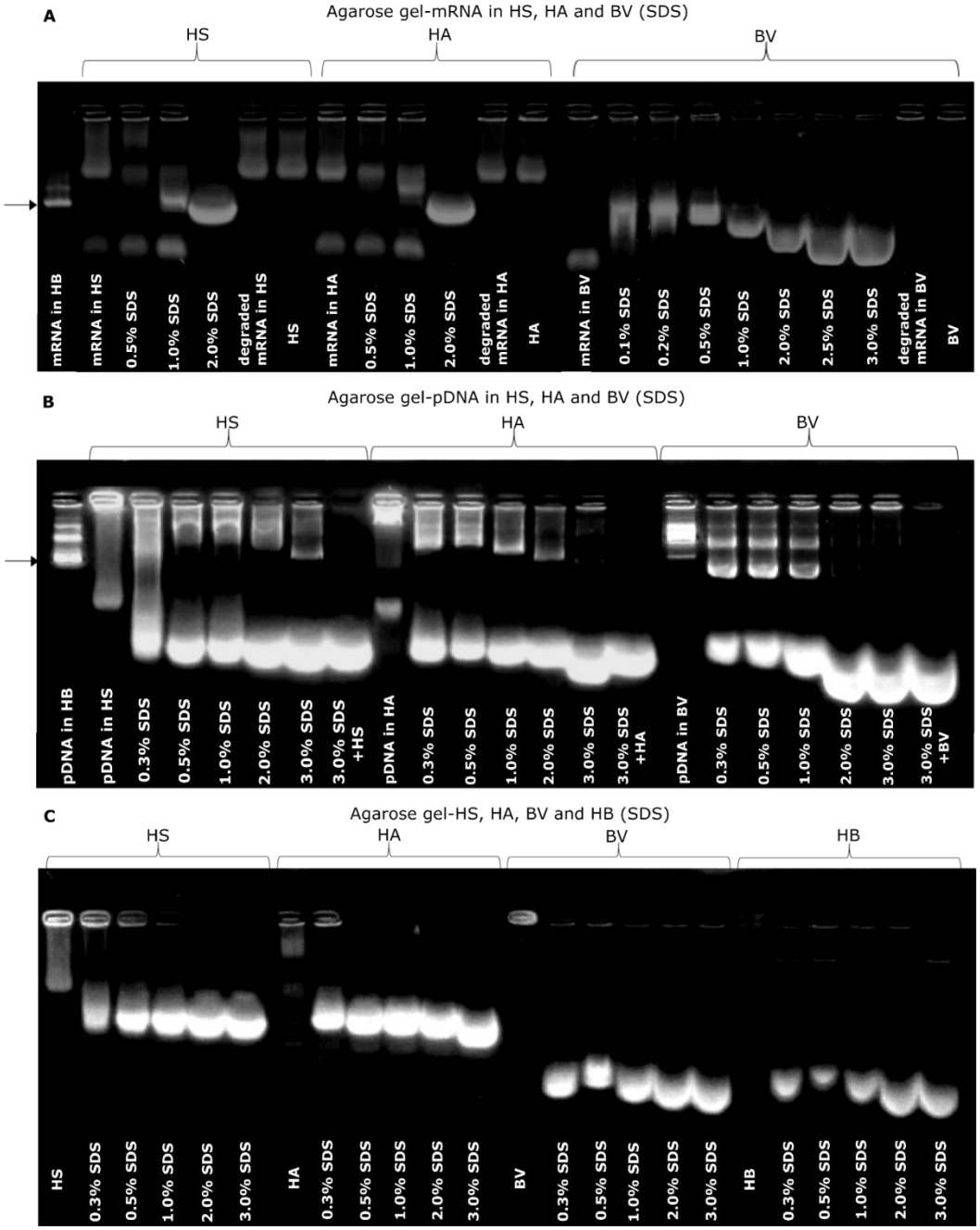

Figure S7. SDS decreased the (A) naked mRNA and (B) naked pDNA degradation in human serum (HS), human ascites (HA) and bovine vitreous (BV). (C) The background induced by SDS on the agarose gel was examined by running the samples only containing human serum, human ascites, bovine vitreous and HEPES buffer with varying amount of SDS. All the experiments were performed for three independent times.

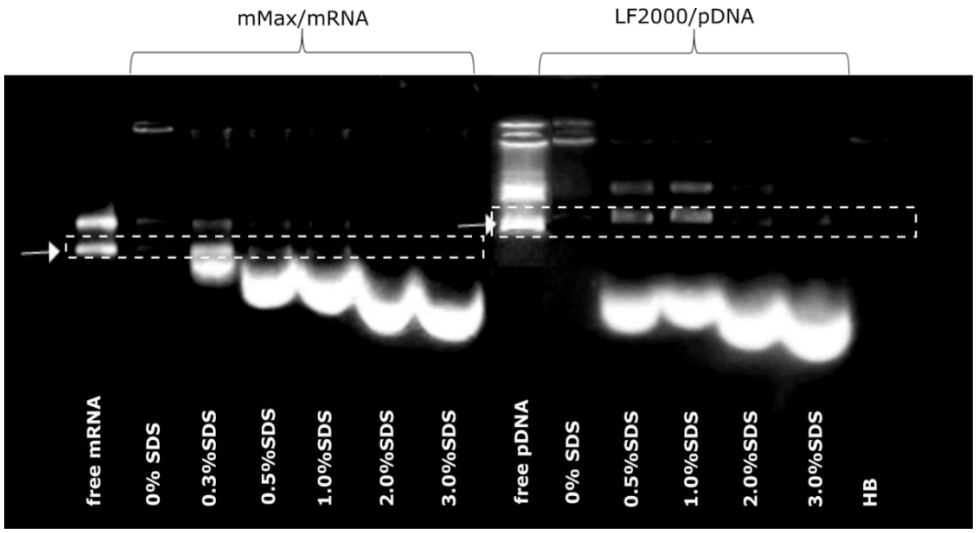

Figure S8. The addition of SDS induced release of mRNA and pDNA from mMax/mRNA complexes and LF2000/pDNA complexes in HEPES buffer, respectively. Complexes were prepared at v/w ratio of 3 according to the protocol provided by the manufacturer. Different amount of SDS was incubated with complexes for 20 min at room temperature before loading on the 1% agarose gel. Free mRNA or pDNA with the same amount as the mRNA present in the complexes was used as control to examine the release of mRNA or pDNA from complexes. All the experiments were performed for three independent times.

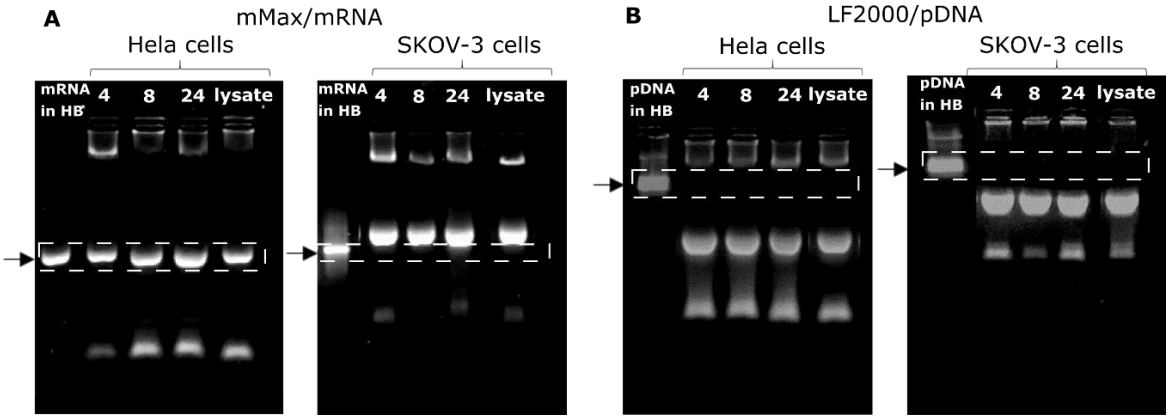

Figure S9. Representative gel of (A) mMax/mRNA and (B) LF2000/pDNA in Hela and SKOV-3 cell lysate. Complexes of mMax/mRNA and LF2000/pDNA were added to Hela and SKOV-3 cells. After 4 hours' incubation, cells were rinsed by DPBS[-] twice and cultured in fresh culture medium. At the end of incubation (4, 8 or 24 h), the cell lysate was harvested and then incubated with SDS for 20 min (final vol. 3%) at room temperature before loading on 1% agarose gel. Intact Cy5 mRNA and Cy5 pDNA (200 ng) was diluted in HEPES buffer and cell lysate alone for loading on the gel as control.

Tables-decay kinetics of mRNA and pDNA by nucleases and biological samples, as calculated from one phase decay using GraphPad Prism. The half-life is presented in minutes or hours. The plateau value shows at which percentage of intact mRNA or pDNA, the decay curve levels off at infinity. Both parameters are used to estimate the degradation of mRNA or pDNA over time, where the half-life indicates the time to decay to halfway the plateau value.

Table 1. Naked mRNA degradation by RNase A followed by gel electrophoresis

RNase A (U/µg mRNA)	0.01	0.03	0.2	0.3
K (min^{-1})	0.014	0.14	2.08	3.13
Half-life (min)	50.98	4.89	0.33	0.22
R^2	0.7660	0.6920	0.9944	0.9710
Plateau	18.42	45.21	2.71	4.74

Table 2. Naked mRNA degradation by RNase A followed by FCS

RNase A (U/µg mRNA)	0.01	0.03	0.2	0.3
K (min^{-1})	3745	0.24	0.52	0.78
Half-life (min)	0.0002	2.89	1.34	0.89
R^2	0.1204	0.7220	0.9363	0.9694
Plateau	93.22	42.71	17.87	6.95

Table 3. Naked pDNA degradation by DNase I followed by gel electrophoresis

DNase I (U/µg pDNA)	0.06	0.1	0.2	0.3
K (h^{-1})	0.18	0.22	0.84	1.71
Half-life (h)	3.76	3.20	0.83	0.41
R^2	0.3555	0.8696	0.8183	0.9172
Plateau	74.84	44.77	16.14	12.22

Table 4. Naked pDNA degradation by DNase I followed by SPT

DNase I (U/µg pDNA)	0.06	0.1	0.2	0.3
K (h^{-1})	0.14	0.071	0.066	0.12
Half-life (h)	5.08	9.40	10.46	6.02
R^2	0.3975	0.8381	0.7260	0.8973
Plateau	70.9	30.12	21.74	5.32

Table 5. Naked mRNA and mRNA complexes degradation followed by FCS

	mRNA (min)				mMax/mRNA (h)			
BF	HB	HA	HS	BV	HB	HA	HS	BV
K (min^{-1} or h^{-1})	0.022	0.62	0.64	0.63	$1.41x10^{34}$	0.25	0.27	0.039
Half-life (min or h)	31.3	1.12	1.09	1.10	$1.41x10^{-35}$	2.74	2.62	17.89
R^2	0.1110	0.9771	0.9821	0.9739	0.1160	0.8374	0.7527	0.7488
Plateau	100.7	22.04	27.15	13.81	93.73	27.87	26.04	32.49

Table 6. Naked pDNA and pDNA complexes degradation followed by SPT

	pDNA (h)				LF2000/pDNA (h)			
BF	HB	HA	HS	BV	HB	HA	HS	BV
K (h^{-1})	0.61	0.75	0.19	0.21	0.26	0.062	0.27	0.51
Half-life (h)	1.14	0.92	3.71	3.31	2.68	11.13	2.56	1.35
R^2	0.6974	0.9151	0.8070	0.9606	0.9443	0.8326	0.9350	0.9012
Plateau	68.23	6.88	65.16	-16.83	9.37	-19.61	12.51	19.78

Biographies

Prof. Dr. Katrien Remaut received her doctor degree in Pharmaceutical Science in the Lab of General Biochemistry and Physical Pharmacy (Ghent University) in 2007, and continued research work as a postdoctoral fellow of the Research Foundation Flanders. In 2013, she was elected as member of the Young Academy in Flanders, and appointed tenure track professor at the same lab of Ghent University in 2014. Her research focuses on ocular gene delivery and peritoneal carcinomatosis, with a special interest into the use of advanced microscopy methods to follow the degradation of nucleic acids during the different steps of the delivery pathway.

Prof. Dr. Kevin Braeckmans obtained a Licentiate degree in Physics in 1999 and a PhD in Pharmaceutical Sciences in 2004 at Ghent University. In 2008 he was appointed as assistant-professor at Ghent University, leading the Bio-Photonic Research Group in close collaboration with the Ghent Research Group on Nanomedicines. At present he is a full professor at Ghent University and a Guest professor at the University of Lille. He focuses on biological barriers to nanomedicines, apart from doing research on light-triggered drug delivery. For this work he was awarded a prestigious ERC Consolidator Grant in 2015 (NANOBUBBLE, 2015-2020).

Prof. Dr. Stefaan C. De Smedt graduated from Ghent University in 1995 and joined the pharmaceutical development group of Janssen Research Foundation (1995-1997). Following post-doctoral research at the Departments of Pharmacy in Ghent and Utrecht he became Professor in Physical Pharmacy and Biopharmacy at Ghent University in 1999 where he founded the Ghent Research Group on Nanomedicines. In 2015, he became Editor of JCR for the region Europe-Middle East & Africa. His research is situated at the interface between drug delivery, material sciences, physical chemistry and biophysics.